Niemann-Pick disease, I-cell disease, and, in particular, AD (Cataldo *et al.* 1997; Mathews *et al.* 2002; Tomiyama *et al.* 2004; Kar *et al.* 2006; Waguri *et al.* 2006). One of the principal pathological hallmarks of AD is the deposition of amyloid β (Aβ), in the form of senile plaques, throughout the hippocampus and neocortex. Aβ is derived from the amyloid precursor protein (APP), and is formed by the sequential cleavage of APP by the β- and γ-secretase enzymes (Saido & Iwata 2006). The localization of β-site APP-cleaving enzyme 1 (BACE1), which is a transmembrane protease with β-secretase activity, is regulated by an acidic-cluster di-leucine motif, which is recognized by Golgi-localized, γ-ear-containing, ADP-ribosylation factor binding protein (Shiba *et al.* 2004; He *et al.* 2005; Tesco *et al.* 2007). Golgi-localized, γ-ear-containing, ADP-ribosylation factor binding protein also plays a crucial role in the trafficking of CI-M6PR. In addition, knockdown by RNA interference (RNAi) of the vacuolar protein sorting protein VPS26, which is another regulator of CI-M6PR transport, has been reported to induce an increased secretion of Aβ40 (Small *et al.* 2005). Therefore, we predicted that kinases that perturb the vesicular transport of CI-M6PR between the endosomes and the TGN would modulate the extent of Aβ secretion.

In this article, we have used cell array chips and gene silencing by RNAi, in combination with visual assays, to establish a two-step functional screening system for human kinases, or their regulators, that might be involved in the localization or shuttling of CI-M6PR. Using this method, we identified five candidate kinases. Furthermore, we found that knockdown of PRKACG (protein kinase, cAMP-dependent, catalytic, gamma) or glycogen synthase kinase 3β (GSK3β), which were two of the five candidates, induced the extensive production of secreted Aβ, and concurrently perturbed the intracellular distribution of BACE1. These results indicated that decreased activity of these two kinases is a possible risk factor for AD. In addition, we found that a functional defect in cytoplasmic linker protein-associating protein 2 (CLASP2), which arose due to the modulation of GSK3β activity, perturbed membrane trafficking between the endosomes and the TGN, and resulted in the mislocalization of BACE1 and extensive Aβ secretion.

Results

Strategy for clarifying the causal connections between the localization of a given protein and the pathogenic mechanism of a related disease

The scheme for our screening and analysis is shown in Fig. 1. To identify human kinases that might be involved in the localization or shuttling of CI-M6PR, we used fluorescence imaging to monitor changes in the localization of CI-M6PR. Immunofluorescence analysis showed an extensive co-localization of CI-M6PR with p230, which is a marker of the TGN, under normal conditions in HeLa cells (Fig. 1A, control). However, if shuttling is perturbed using an appropriate kinase inhibitor or an siRNA against a particular kinase, CI-M6PR that is being recycled will be trapped in the early/late endosomes or at the plasma membrane (PM). As a result, the fluorescence signal from CI-M6PR becomes dispersed throughout the cytoplasmic endosomes and no longer overlaps with that of p230. The morphology of the Golgi, however, is virtually unaffected, as shown by the staining pattern of p230. For example, treatment of HeLa cells with 3-methyladenine (3-MA), which is a specific inhibitor of the class III phosphoinositide 3-kinase (PI3K) and is known to inhibit retrograde transport from early endosomes to the TGN, resulted in a dispersed signal for CI-M6PR that did not co-localize with that of p230 (Fig. 1A, Perturbation of transport by 3-MA) (Hirosako *et al.* 2004).

In practice, for the first round of screening, we screened kinase inhibitors to identify those that disrupted the localization of CI-M6PR (Fig. 1B, kinase inhibitor screening). A kinase inhibitor usually inhibits several types of kinase at its different concentrations. For example, Bisindolylmaleimide (BIM) at the concentration approximately 10 nM inhibits a protein kinase C (PKC) but it also inhibits protein kinase A (PKA) at high concentrations more than 2 μM. Taking the concentration-dependent broad specificity of kinase inhibitors into consideration, we carried out the kinase inhibitor screening at four different concentrations. The concentration for each kinase inhibitors were described in Table S1 in Supporting Information. In the second round of screening, we used the results of the first round to design RNAi experiments that would allow us to identify specific kinases or kinase regulators that were responsible for the phenotypes of interest (Fig. 1B, kinase siRNA screening).

To allow the imaging of as many samples as possible for large-scale screening applications and to acquire numerous imaging data in a systematic manner, we developed an automated high-throughput fluorescence-based cell imaging system using cell array chips. The system consisted of microchamber array chips, an automatic pipetting device (Fig. 1B, the CellTech Station, which was custom-made for us by Nikkyo Technos Co., Ltd), and an automatic system for the capture of fluorescent images. We used two types of imaging tool: an INCell Analyzer 1000 system (GE Healthcare Co., Ltd) and an LSM510 laser scanning confocal microscope (Carl Zeiss, Co., Ltd).

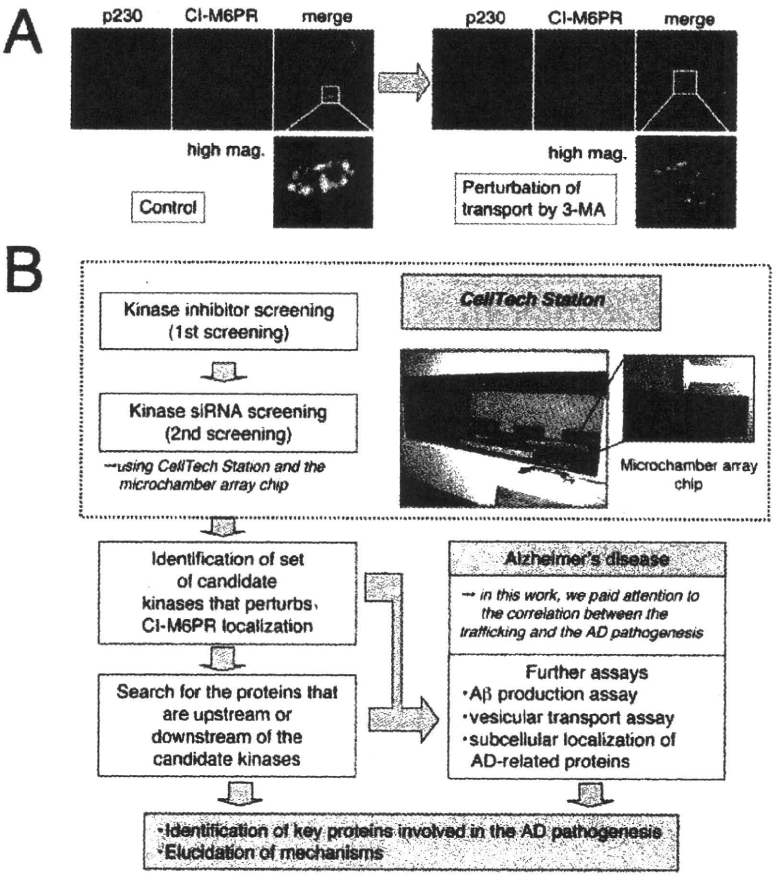

Figure 1 Flowchart for the identification of kinase-regulated pathways for the trafficking of CI-M6PR by high-throughput visual screening.

After identification of candidate kinases that perturbs CI-M6PR localization, we are going to investigate the relation between the defect in the trafficking of CI-M6PR and the AD pathogenesis using biochemical and cell biological studies (Fig. 1B, a panels on the bottom-right corner). Concurrently, we are going to search for the proteins that are upstream or downstream of the candidate kinases using available database or literature information network, and examine the role of the protein in the AD pathogenesis (Fig. 1B, a panel on the bottom-left corner). Considering all the protein information obtained above together, we are going to identify the key protein(s) involved in the AD pathogenesis.

Identification of kinase inhibitors that perturb CI-M6PR localization and TGN morphology

To determine the types of kinase that affect the intracellular localization of CI-M6PR or TGN morphology, we examined the effect of 29 different kinase inhibitors (Table S1 in Supporting Information) on the localization of CI-M6PR using our cell array chip-based automatic screening system. HeLa cells were first incubated with various kinase inhibitors in microchambers, and then fixed and immunostained with antibodies against p230 and CI-M6PR. Images were acquired using the INCell Analyzer 1000 or LSM510 confocal microscope, and the co-localization of CI-M6PR fluorescence (red) and p230 fluorescence (green) was analyzed by means of the co-localization index that is described in Fig. 2.

We identified the following five kinase inhibitors that disrupt the localization of CI-M6PR: Bisindolylmaleimide I (BIM) (Lee *et al.* 2005), SH-5 (Kierbel *et al.* 2005), staurosporine (Dangi & Shapiro 2005), GSK3β kinase inhibitor VII (Conde *et al.* 2003), and *4,5,6,7*-Tetrabromobenzotriazole (TBB) (Schermer *et al.* 2005). When HeLa cells were treated with these kinase inhibitors, with the exception of GSK3β kinase inhibitor VII, CI-M6PR became localized to punctate cytoplasmic structures, which are probably endosomal compartments, rather than

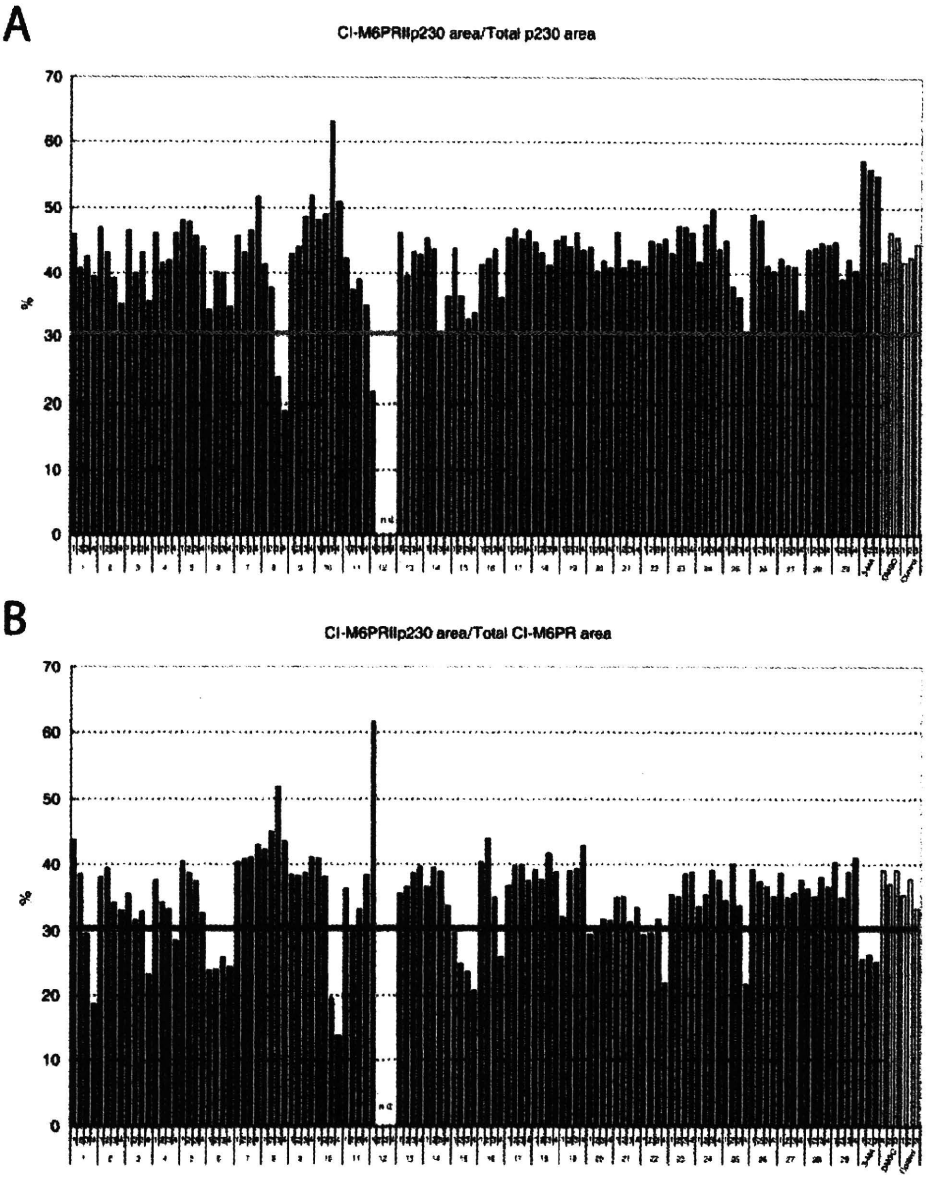

Figure 2 Co-localization index used in our visual screening to identify kinase inhibitors that perturb CI-M6PR localization in HeLa cells. (A) HeLa cells were treated with the kinase inhibitors that are listed in Table S1 in Supporting Information. We carried out immunostaining using antibodies against CI-M6PR and p230, and calculated the area in which CI-M6PR co-localized with p230 using the InCell Analyzer. The graph shows the percentage of the p230-positive area in which CI-M6PR is detected. The kinase inhibitors that gave a value of < 30% are Roscovitine (8) and JNK inhibitor II (12). (B) HeLa cells were treated with the kinase inhibitors at three different concentrations described in Table S1 in Supporting Information, and immunostained as described above. The graph shows the percentage of the CI-M6PR-positive area in which p230 is detected. Kinase inhibitors that gave a value of < 30% are as follows: H-89 (1), BIM (3), SH-5 (4), STS (6), Genistein (10), GSK3β VII (11), TBB (16), JNK inhibitor II (12), AG1296 (15), Calphostin C (22), and Sphingosine kinase inhibitor (25). We analyzed the fluorescent images of cells that had been treated with each kinase inhibitor, and found that the color of the inhibitors affected the measurements for 8, 12, and 22. In addition, the p230-positive Golgi apparatus was disrupted in 1, 10, 15, and 25. Taken together, we identified five kinase inhibitors that affect the localization of CI-M6PR, but not p230: BIM (3), SH-5 (4), STS (6), GSK3 β inhibitor VII (11), TBB (16). Red bar = 3-MA as a positive control; Yellow bar = DMSO; White bar = a negative control.

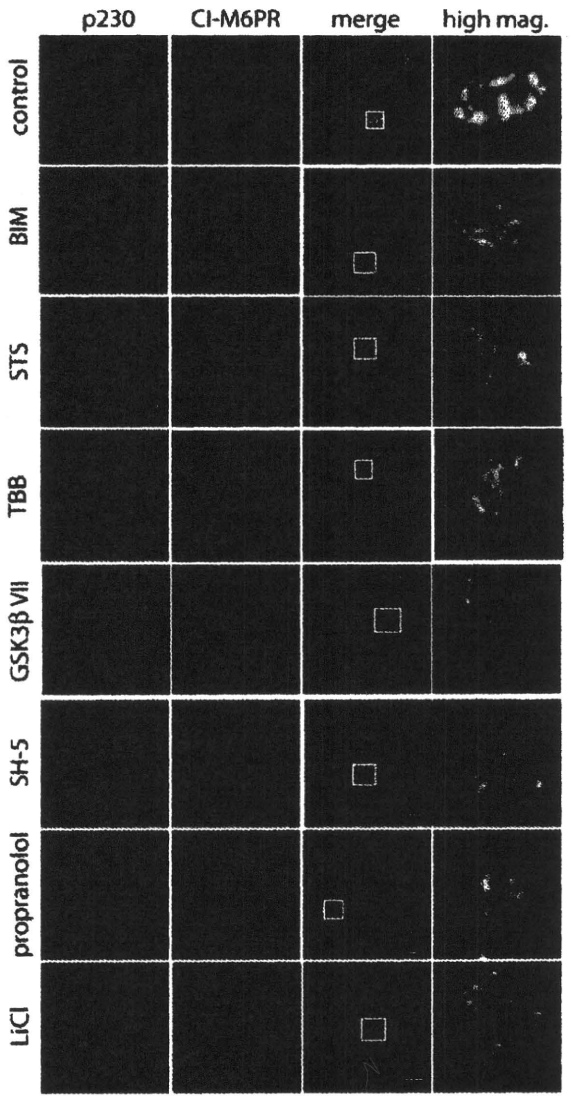

Figure 3 Validation of kinase inhibitors that perturb CI-M6PR localization in HeLa cells. HeLa cells that had been grown in microchambers were incubated in the presence of DMSO (14 mM, control) for 3 h, BIM (20 μM, BIM) for 0.5 h, staurosporine (2 μM, STS) for 2 h, TBB (200 nM, TBB) for 3 h, GSK-3β kinase inhibitor VII (50 μM, GSK3β VII) for 0.5 h, or SH-5 (10 μM, SH-5) for 2 h. HeLa cells that had been cultured in glass-based dishes were incubated with propranolol (100 μM, propranolol) for 1 h, or LiCl (20 mM, LiCl) for 3 h. After incubation, the cells in either the microchambers or the glass-based dishes were fixed and incubated with anti-p230 and anti-CI-M6PR antibodies, followed by Cy2- or Cy3-conjugated secondary antibodies, respectively. The samples were viewed using an LSM510 confocal microscope with a 63x Plan-Neofluar oil immersion objective.

to the TGN (Fig. 3). However, the localization of p230 did not change. BIM is a PKC inhibitor that also inhibits protein kinase A (PKA) at high concentrations (≥ 2 μM). Propranolol, which is another PKA inhibitor, resulted in the localization of CI-M6PR in punctate cytoplasmic structures rather than in the TGN (Fig. 3, Propranolol) (Saucerman *et al.* 2006). Staurosporine is a broad spectrum inhibitor of protein kinases. The cells appeared to become more rounded after treatment with staurosporine, but the localization of CI-M6PR changed in a similar manner to that seen with the other inhibitors. TBB is a specific casein kinase II (CK2) inhibitor. The retrieval of CI-M6PR from the endosomes to the TGN was reported to be controlled by the phosphorylation of phosphofurin acidic cluster sorting protein 1 (PACS-1) by CK2 (Scott *et al.* 2006). GSK3β kinase inhibitor VII is a specific inhibitor of GSK3β kinase, and caused fragmentation of the TGN and the apparent partial segregation of the two markers (Fig. 3; GSK3β kinase inhibitor VII). The same phenotype was observed after treatment with LiCl, another GSK3β inhibitor (Fig. 3; LiCl) (Cheng *et al.* 2008). As a result, we chose three types of kinase for the subsequent RNAi experiments: protein kinases of the AGC group, CK2, and GSK3β.

Identification of kinases that are involved in CI-M6PR localization

Next, we examined the effect of siRNAs (*Silencer* Human Kinase siRNA Library; Ambion) for 80 kinase genes (AGC group, 76 genes; CK2, 3 genes; GSK3β, 1 gene; the names of the kinases are given in Table S2 in Supporting Information) on CI-M6PR localization/sorting using our automatic visual screening system with the LSM510 confocal microscope as the imaging system. With our RNAi system, the efficiency of gene silencing in HeLa cells was found to be more than 90%, as measured morphologically by the knockdown of kinesin family member 11 (KIF11) (Fig. S1 in Supporting Information). We identified five kinases whose knockdown perturbed the localization of CI-M6PR: CDC42 binding protein kinase-β (CDC42BPB), protein kinase, cAMP-dependent, catalytic-α (PRKACA), protein kinase, cAMP-dependent, catalytic-γ (PRKACG), GSK3β, and CSNK2A1 (casein kinase 2, alpha 1 polypeptide).

CDC42BPB regulates cell polarity by controlling the dynamics of actin and myosin (Gomes *et al.* 2005; Wilkinson *et al.* 2005). PRKACA and PRKACG are catalytic subunits of PKA, which regulates the dynamics of many organelles through its interaction with A-kinase anchoring protein (Wong & Scott 2004). GSK3β regulates microtubule dynamics and cellular responses, including

protein synthesis, gene expression, and protein degradation (Akhmanova *et al.* 2001; Fumoto *et al.* 2006). CSNK2A1 is one of the subunits of CK2, which was reported to regulate CI-M6PR trafficking in HeLa cells (Scott *et al.* 2006). We confirmed that the protein levels of these five kinases were reduced in the cells that had been transfected with the appropriate siRNAs compared to those in cells that had been transfected with an siRNA against enhanced green fluorescent protein (eGFP) (Fig. S2A in Supporting Information).

Gene silencing of CDC42BPB induced the redistribution of CI-M6PR from the TGN to cytoplasmic structures (Fig. 4, CDC42BPB), but also resulted in the partial disruption of the Golgi apparatus. Gene silencing of PRKACA, PRKACG or CSNK2A1 changed the localization of CI-M6PR from the TGN to cytoplasmic structures (Fig. 4, PRKACA, PRKACG, CSNK2A1). GSK3β knockdown caused the fragmentation of the TGN that contained both CI-M6PR and p230 (Fig. 4, GSK3B).

We examined the co-localization of CI-M6PR with various organelle markers in kinase-knockdown HeLa cells by immunofluorescence. The following organelle markers were used: EEA1 (early endosome antigen 1) as an early endosome marker, 2,2′-dioleoyl lysobisphosphatidic acid (LBPA) as a late endosome marker, and Lamp2 as a lysosomal marker. In control HeLa cells, none of the organelle markers (EEA1, LBPA and Lamp2) overlapped with the CI-M6PR-positive punctate structures (Fig. S3, B and C; control in Supporting Information). In these cells, CI-M6PR localized primarily to the TGN and to specialized vesicles, but not to the early/late endosomes as had been shown in another report (Hirosako *et al.* 2004). In the knockdown cells, CI-M6PR co-localized partially with EEA1 in the peripheral cytoplasmic vesicles, but not with the other markers (Fig. S3A–C in Supporting Information). The change in localization of CI-M6PR in the GSK3β-knockdown cells was of particular interest. In these cells, the majority of the fluorescent signal for all the marker proteins appeared to be clustered in the central region of the cells, near the centrosome. CI-M6PR co-localized partially with EEA1 and LBPA in this central region in the knockdown cells (Fig. S3A–C; GSK3B in Supporting Information).

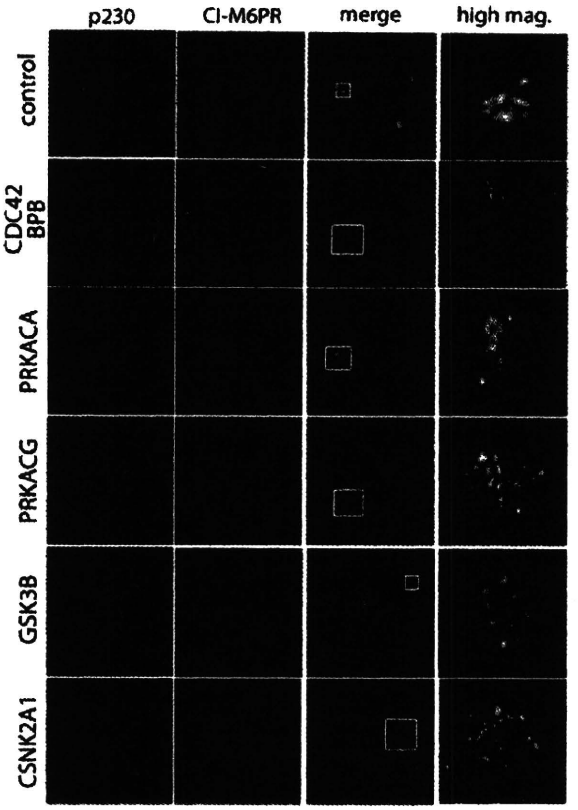

Figure 4 Visual screening to identify kinase siRNAs that perturb CI-M6PR localization in HeLa cells. HeLa cells that had been grown in microchambers were transfected with 50 nM siRNA against a control protein (eGFP), or against CDC42BPB, PRKACA, PRKACG, GSK3β, or CSNK2A1. After incubation for 72 h in culture medium, the cells were fixed and incubated with anti-p230 and anti-CI-M6PR antibodies, which were visualized by Cy2- and Cy3-conjugated secondary antibodies, respectively. The samples were viewed using an LSM510 confocal microscope with a 63x Plan-Neofluar oil immersion objective. Bar = 10 μm.

Effects of gene silencing of the identified kinases on APP processing

We next investigated the relation between the perturbations in the trafficking of CI-M6PR that were induced by kinase knockdown and the pathogenic processing of Aβ using HEK-APP cells, which stably express Swedish mutant APP (APPsw). We confirmed that the protein level of each kinase was decreased in the kinase-knockdown cells (Fig. S2B in Supporting Information).

Initially, to detect the final products of APP processing, we measured the amount of Aβ40 and Aβ42 that had been secreted into the medium using a sandwich ELISA. Gene silencing of PRKACG and GSK3β increased the amounts of secreted Aβ40 and Aβ42 by approximately twofold in both cases, compared with that secreted by the control cells (Fig. 5A). Gene silencing of the other kinases had no effect on the amount of Aβ40 or Aβ42 that was secreted.

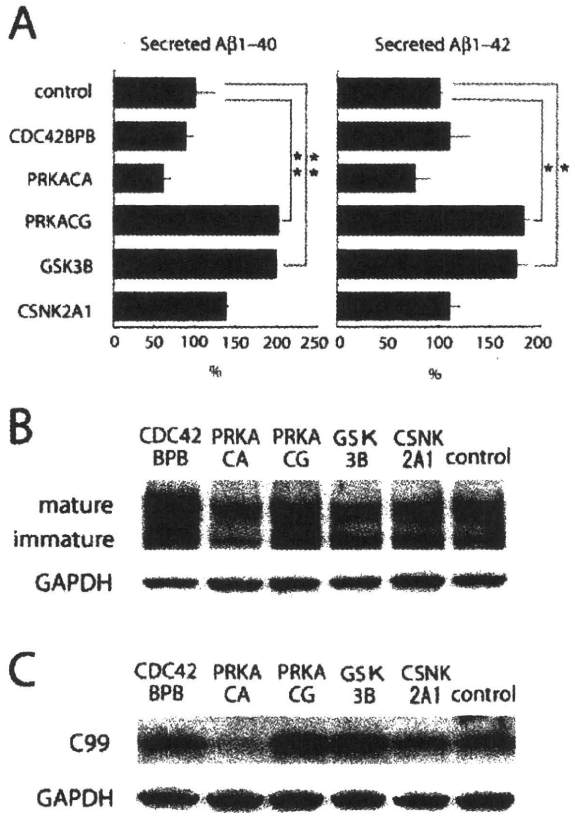

Figure 5 Effects of kinase knockdown on the secretion of Aβ40 or Aβ42 into the medium (A), APP maturation (B), or β-secretase activity (C). (A) HEK-APP cells were plated on poly-L-lysine-coated 6-well plates and transfected with 50 nM siRNA for each kinase indicated. After incubation for 72 h, the medium was replaced with fresh medium. Six hours after the medium was exchanged, the medium and cells were collected. The levels of secreted Aβ40 and Aβ42 in the medium were measured by ELISA and normalized against the concentration of protein in the cell lysate. Values are means ± S.E.; $n = 3$, $*P < 0.05$, $**P < 0.005$, *t*-test. (B) After incubation for 72 h, the cells were lysed and the cell proteins immunoblotted using a mouse monoclonal antibody (AB5352) against the C-terminus of APP to detect APP maturation. (C) After incubation for 72 h, the cells were lysed and cell proteins immunoblotted using a monoclonal antibody (82E1) against the N-terminus of human Aβ to detect the C99 fragment. GAPDH was used as a loading control for both experiments.

Next, we examined the maturation of APP in HEK-APP cells by Western blotting. With the lysate from the control cells, both the mature form and the immature form of APP were detected on the western blot. The immature form of APP is predominantly *N*-glycosylated and localized in the endoplasmic reticulum (ER) and the *cis*-Golgi. The mature form is an *N*,*O*-glycosylated species that is concentrated in the TGN/PM (Weidemann *et al.* 1989). Gene silencing of CDC42BPB or PRKACG resulted in an increase in the level of the mature form (Fig. 5B). In contrast, the knockdown of PRKACA caused a reduction in the total amount of APP protein. Gene silencing of GSK3β or CSNK2A1 had no effect on the maturation compared with that in control cells (Fig. 5B, GSK3B and CSNK2A1).

Finally, we examined β-secretase activity in the cells. The activity was estimated by measuring the amount of the APP C-terminal C99 fragment, which is produced by β-secretase, in the cells. The C99 fragment was detected by Western blotting with the 82E1 monoclonal antibody, which reacts with the C99 fragment but does not react with the APP C-terminal fragment that is produced by α-secretase. We found that gene silencing of PRKACG or GSK3β increased the level of the C99 fragment compared with that in control cells. Taken together with the results of the APP processing experiments, we concluded that the knockdown of PRKACG or GSK3β induced a substantial increase in Aβ secretion. It remains possible that the other kinases (CDC42BPB, PRKACA and CSNK2A1) that have been implicated in CI-M6PR trafficking could be involved in the pathogenesis of CI-M6PR-related diseases other than AD.

Next we examined the subcellular localization of the AD-related protein, BACE1, in PRKACG- and GSK3β-knockdown cells because there had been many reports that suggested a positive correlation between the perturbation of membrane trafficking of BACE1 and the pathogenesis of AD, and because CI-M6PR and BACE1 contain the same sorting signal in their cytoplasmic region (Shiba *et al.* 2004; He *et al.* 2005; Tesco *et al.* 2007). To monitor the localization of BACE1, we expressed myc-tagged BACE1 protein in HeLa cells, and carried out indirect immunofluorescence analysis using an anti-myc antibody. In control cells, BACE1 localized mainly to the juxtanuclear region and partially to the PM. We found by dual-immunofluorescence analysis that BACE1 co-localized with EEA1 in the juxtanuclear region, but not in the cytoplasmic vesicles (Fig. 6, control). In contrast, in PRKACG-knockdown cells, the majority of the BACE1 was localized not in the juxtanuclear region but in cytoplasmic vesicles, where it partially co-localized with EEA1 (Fig. 6, PRKACG). In the GSK3β-knockdown cells, almost all the fluorescent signal from BACE1 co-localized with that from EEA1, and the BACE1/EEA1-positive vesicles appeared to be clustered in the central region of the cells, near the centrosome (Fig. 6, GSK3B), as was the signal from CI-M6PR.

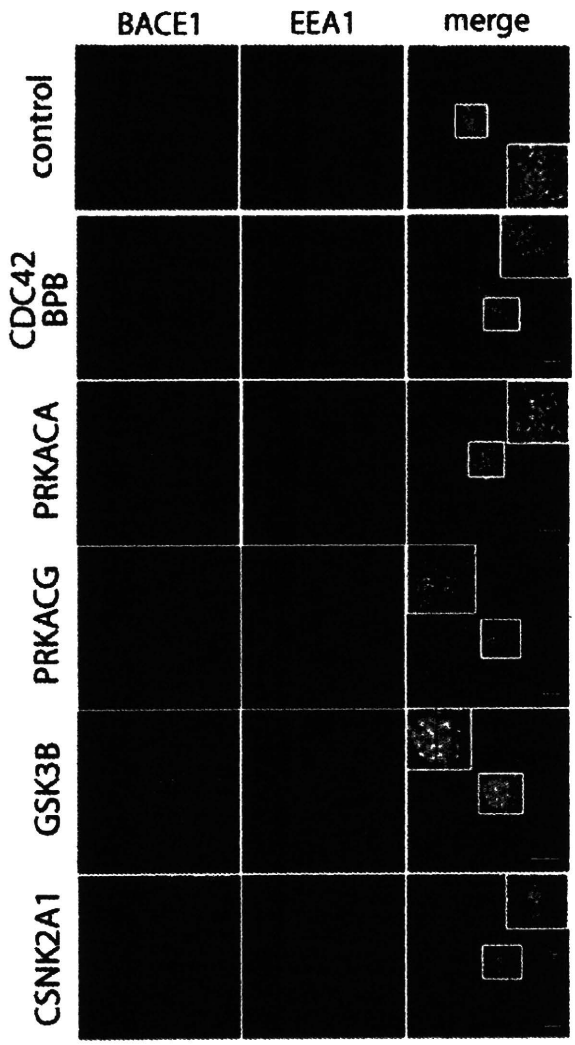

Figure 6 Changes in the subcellular localization of BACE1 and EEA1 in kinase-knockdown HeLa cells. HeLa cells that had been grown on glass-based dishes were transfected with 50 nM siRNA against a control protein (eGFP), PRKACG, or GSK3β. The cells were further transfected with 1 μg/mL BACE1-myc plasmid at 48 h after transfection with the siRNAs. After further incubation for 24 h, the cells were fixed and dual-immunostained with anti-myc and anti-EEA1 antibodies, followed by Alexa 488- or Cy3-conjugated secondary antibodies, respectively. The samples were viewed using an LSM510 confocal microscope with a 63x Plan-Neofluar oil immersion objective. Scale bar = 10 μm.

Functional modulation of CLASP2 by GSK3β is involved in Aβ secretion

To investigate the relation between GSK3β or PRKACG knockdown and increased Aβ secretion, we searched for proteins whose function is regulated by the kinases and that are involved in the vesicular transport between endosomes and the TGN.

As a result, we focused on the function of CLASP2, which is a microtubule binding protein (Efimov *et al.* 2007). CLASP2 contains several potential GSK3β phosphorylation motifs and its function could be regulated by GSK3β. CLASP2 associates specifically with the TGN protein GCC185 and functions in the formation of the asymmetric microtubule network in polarized cells. GCC185 was found to play a crucial role both in the retrograde transport of Shiga toxin and CI-M6PR between the recycling endosomes and the TGN, and in the maintenance of Golgi morphology (Akhmanova *et al.* 2001; Mimori-Kiyosue *et al.* 2005; Wittmann & Waterman-Storer 2005; Reddy *et al.* 2006; Derby *et al.* 2007). In contrast to GSK3β, we could not find any relation between PRKACG and the AD even if we searched for a relationship using the available databases.

First we examined the relation between GSK3β activity and CLASP2 function. We found that GSK3β knockdown reduced the number of centrosomally focused microtubules (oriented microtubule networks around the centrosome) and simultaneously induced a slight fragmentation of the Golgi apparatus (Fig. 7A) as reported previously (Fumoto *et al.* 2006). We also found that CLASP2-knockdown cells showed the same morphological phenotypes with regard to the centrosomal microtubules but the morphology of the Golgi remained intact (Fig. 7A). CLASP2, which accumulated at the TGN in control cells, dissociated substantially from the fragmented Golgi membranes in GSK3β-knockdown cells (Fig. 7B). In addition, we detected a substantial inhibitory effect on CLASP2 phosphorylation in GSK3β-knockdown or lithium chloride-treated cells (Fig. 7D). These results suggest that a decrease in GSK3β activity could modulate the localization of CLASP2 to the TGN and its function.

Next we examined the effects of the knockdown of CLASP2 on either the anterograde transport of a temperature sensitive version of the vesicular stomatitis virus glycoprotein (VSVGts045) from the ER to the PM or the retrograde transport of Cholera Toxin subunit B (CTxB) from the endosome to the TGN. The knockdown had no effect on the anterograde transport of VSVGts045-GFP (Adachi *et al.*, unpublished data) but caused substantial retardation of the retrograde transport of CTxB (Fig. S4B, siRNA CLASP2 in Supporting Information). A similar delay in the transport was observed in GSK3β-knockdown cells (Fig. S4A in Supporting Information, siRNA GSK3B). The localization of BACE1 in the CLASP2-knockdown cells was perturbed in a similar manner as in the GSK3β-knockdown cells

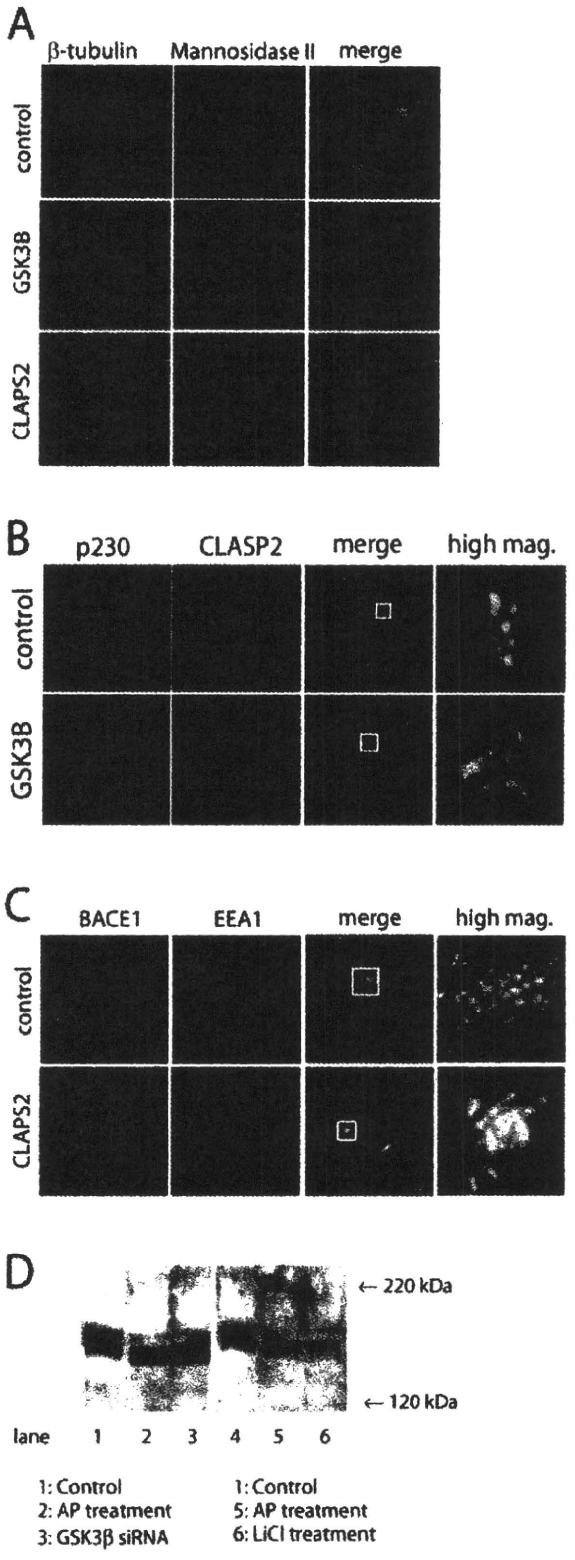

(Fig. 7C). Finally, we measured the secretion of Aβ40 and Aβ42 into the medium. CLASP2 knockdown increased the amounts of secreted Aβ40 and Aβ42 by approximately 2.0-fold and 1.4-fold, respectively, as compared with the control (Fig. 8A). These results suggested that a decrease in GSK3β activity might modulate the activity of CLASP2 in microtubule dynamics or in the TGN, which would in turn result in the mislocalization of BACE1 and an extensive secretion of Aβ.

We compared the coalescence of APP and BACE1 in GSK3β- or CLASP2-knockdown cells to that in control cells morphologically using an immunofluorescence

Figure 7 Effects of gene silencing of GSK3β or CLASP2 on the morphology of microtubules and the Golgi apparatus in HeLa cells (A), on the dissociation of CLASP2 from the Golgi membranes (B), on the changes in the subcellular localization of BACE1 and EEA1 (C), or on the phosphorylation states of CLASP2 (D). (A) GSK3β- or CLASP2-knockdown HeLa cells were fixed and dual-immunostained with antibodies against anti-β-tubulin and anti-mannosidase II (medial Golgi marker), followed by Alexa 488- or Cy3-conjugated secondary antibodies, respectively. The samples were viewed using an LSM510 confocal microscope with a 63x Plan-Neofluar oil immersion objective. Scale bar = 10 μm. GSK3β or CLASP2 knockdown reduced centrosomally-focused microtubules (oriented microtubule networks around the centrosome). GSK3β knockdown caused the disassembly of the Golgi apparatus, but CLASP2 knockdown did not. (B) GSK3β knockdown induced a slight fragmentation of the Golgi apparatus, which occurred concomitantly with the dissociation of CLASP2 from the TGN membranes. (C) HeLa cells that had been grown on glass-based dishes were transfected with 50 nM siRNA against a control protein (eGFP) or CLASP2. The cells were further transfected with 1 μg/mL BACE1-myc plasmid at 48 h after transfection with the siRNAs. After further incubation for 24 h, the cells were fixed and dual-immunostained with anti-EEA1 and anti-myc antibodies, followed by Alexa 488- or Cy3-conjugated secondary antibodies, respectively. The samples were viewed using an LSM510 confocal microscope with a 63x Plan-Neofluar oil immersion objective. Scale bar = 10 μm. The localization of BACE1 in CLASP2-knockdown cells was perturbed as had been observed in the GSK3β-knockdown cells (compare with the image in Supporting Information Fig. S6, GSK3B). (D) The inhibition of phosphorylation of CLASP2 in the GSK3β-knockdown HeLa cells was detected by the treatment of cell lysates with alkaline phosphatase (AP). We examined the effect of decreasing the activity of GSK3β by siRNA or lithium chloride on two protein bands. As shown in the figure, two CLASP2-positive bands were observed in HeLa cell lysate (lane 1). Interestingly, the upper band disappeared and shifted to the lower position upon AP treatment (lane 2). The same shift was observed in the lysate of GSK3β-knockdown cells (lane 3). Treatment with lithium chloride also induced the same shift of bands (lane 4, control; lane 5, AP treatment; lane 6, LiCl treatment). Therefore, the upper band of CLASP2 in the blot might correspond to phosphorylated CLASP2.

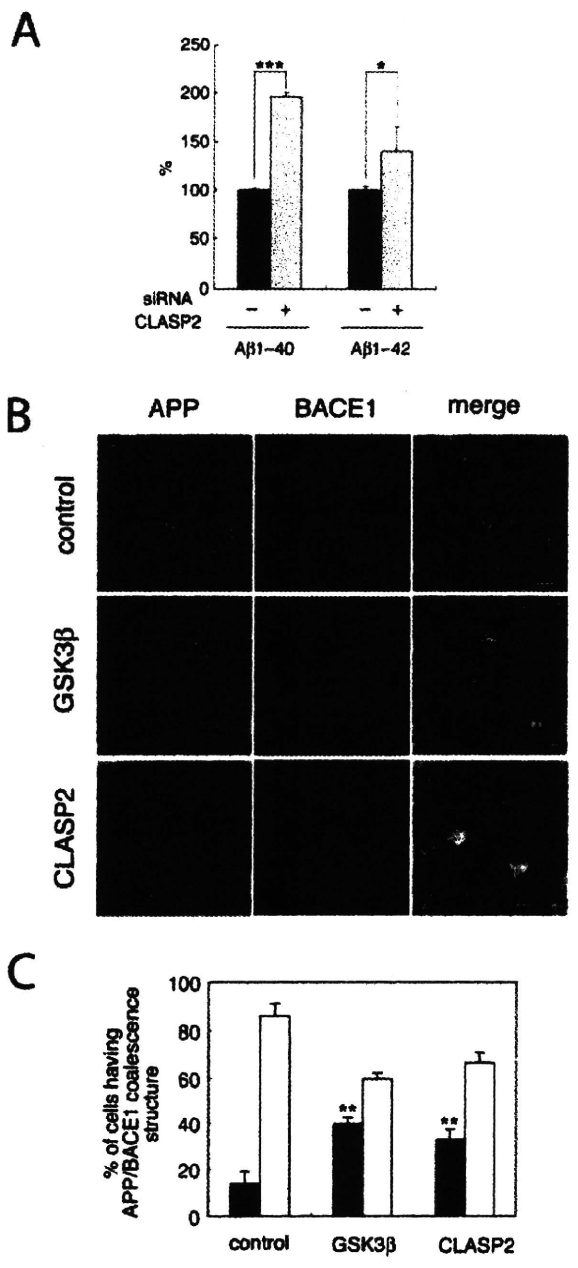

Figure 8 Effects of CLASP2 knockdown on Aβ40 or Aβ42 secretion into the medium (A), or the coalescence of BACE1 and APP in endosomes (B, C). (A) HEK-APP cells were plated on poly-L-lysine-coated 6-well plates and transfected with 50 nM siRNA against CLASP2. After incubation for 72 h, the medium was replaced with fresh medium. Six hours after the medium was exchanged, the medium and cells were collected. The levels of secreted Aβ40 and Aβ42 in the medium were measured by ELISA and normalized against the concentration of protein in the cell lysate. Values are means ± SE; $n = 3$, $*P < 0.05$, $**P < 0.005$, *t*-test. (B) HEK-APP cells that had been grown on glass-based dishes were transfected with 50 nM siRNA against either a control protein (eGFP) or CLASP2. The cells were further transfected with 1 μg/mL BACE1-myc plasmid at 48 h after the initial siRNA transfection. After further incubation for 24 h, the cells were fixed and dual-immunostained with anti-APP and anti-myc antibodies, which were visualized by Alexa 488- or Cy3-conjugated secondary antibodies, respectively. The samples were viewed using an LSM510 confocal microscope with a 63× Plan-Neofluar oil immersion objective. Scale bar = 10 μm. The knockdown of CLASP2 induced the extensive coalescence of APP and BACE1 in the centrosomal region of the cells. (C) The percentage of the cells in which the co-localization of APP and BACE1 was observed was compared with that of the control cells using morphometric analysis. BACE1 in control cells did not co-localize with APP. In contrast, extensive co-localization of these proteins was observed in GSK3β- or CLASP2-knockdown cells. Values are means ± SE; $n = 3$, $*P < 0.05$, $**P < 0.005$, *t*-test.

method. In control cells, BACE1 did not co-localize with APP, rather the fluorescence signal of BACE1 appeared to be segregated completely. In contrast, substantial, but not complete, co-localization of the two fluorescence signals was observed in GSK3β- or CLASP2-knockdown cells (Fig. 8B,C).

Discussion

In this article, we describe the development of a versatile functional screening system to examine the vesicular trafficking of CI-M6PR and its regulating kinase by detecting changes in the localization of the protein. As a result, we identified two kinase-regulated trafficking pathways that were involved in the pathogenesis of AD through the activation of Aβ secretion; a PRKACG-regulated pathway that was associated with aberrant accumulation of matured APP in the cells and a GSK3β-regulated pathway that was associated with the accumulation of BACE1-containing endosomes near the juxtanuclear region.

PKA has been implicated in the pathological hyperphosphorylation of tau on Ser214 and 409, which leads to the formation of neurofibrillary tangles in AD (Wang *et al.* 2007). In addition, Su *et al.* (2003) showed that H-89 (a PKA inhibitor) inhibited the maturation of APP, which involves *O*-glycosylation during a post-Golgi stage of the secretory pathway, and secretion of Aβ. However, the role of PKA during APP processing is not clear. In this study, we demonstrated the silencing of PRKACG, which is a catalytic subunit of PKA, increased the mature form of APP (Fig. 5B) and activated Aβ secretion (Fig. 5C).

GSK3β has been shown to play a crucial role in the phosphorylation of tau and the modulation of APP

processing (Phiel *et al.* 2003; Noble *et al.* 2005; Rockenstein *et al.* 2007; Wang *et al.* 2007), which suggests that abnormal levels and activity of GSK3β may be associated with the pathology of AD. However, there have been very few reports that have examined the relation between GSK3β activity and a specific trafficking pathway for AD-related proteins. This is the first time that a positive relation between a GSK3β-regulated membrane trafficking pathway and Aβ secretion has been demonstrated.

We searched for proteins whose function is regulated by PRKACG or GSK3β and that are involved in the vesicular transport between endosomes and the TGN. We could not find any association between PRKACG and AD even if we searched for a relationship using the available databases. However, we found that a functional defect in CLASP2, which arose due to the modulation of GSK3β activity, might perturb membrane trafficking between the endosomes and the TGN through its deficient interaction with the Golgi associating protein GCC185. Therefore, we attempted to gain further mechanistic insight at a molecular level into how GSK3β and CLASP2 control the specific trafficking pathway that is involved in the pathogenic secretion of Aβ. As a result, we found that the modulation of GSK3β-mediated phosphorylation of CLASP2 resulted in the mislocalization of BACE1 and extensive Aβ secretion (Fig. 8). There has been reported that the modulation of GSK3β-mediated phosphorylation of CLASP2 results in a significant increase in CLASP2 signal at distal microtubule ends (plus ends) and is involved in the local regulation of microtubule dynamics (Akhmanova *et al.* 2001; Wittmann & Waterman-Storer 2005). In addition, we observed that GSK3β-knockdown reduced the number of centrosomally-focused microtubules and induced the sight fragmentation of the Golgi apparatus (Fig. 7A). These results indicate that the modulation of GSK3β-mediated phosphorylation of CLASP2 might cause the defect in the microtubule-dependent membrane trafficking pathways between the Golgi and endosomes. In fact, we observed substantial retardation of the retrograde transport of CTxB from endosomes to the TGN (Fig. S4B in Supporting Information). The defect in the transport pathways might cause an extensive coalescence of APP and BACE1 in the juxtanuclear region of GSK3β- or CLASP2-knockdown cells and result in an extensive Aβ secretion. At this time, we cannot elucidate the causal correlation between the defect in the trafficking pathways and the promotion of coalescence of APP and BACE1. More biochemical studies are needed to solve the issue.

There have been several reports that demonstrated that the inhibition of clathrin-mediated endocytosis reduces β-cleavage of APP and thus Aβ production (Ehehalt *et al.* 2003; Rajendran *et al.* 2006). It was suggested that APP and BACE1 are combined together after endocytosis by the clustering and coalescence of APP- and BACE1-containing rafts within endosomes (Hattori *et al.* 2006). A significant fraction of BACE1 is known to localize to lipid rafts and amyloidogenic processing of APP might occur within these rafts. As shown in Fig. 8(B,C), our immunofluorescence analysis showed that a large extent of fluorescence signal of APP appeared to coalesce with that of BACE1 in GSK3β- or CLASP2-knockdown cells. At this time, we could not clarify whether both APP and BACE1 are in the rafts of "same membrane vesicles". Hattori *et al.* (2006) reported that BACE1 and APP cluster and coalesce each other in the lipid raft at endosomes. As shown in Fig. S3A in Supporting Information, we observed that both BACE1 and APP were in the EEA1-positive membranous structures, suggesting the possibility that the membranous structures, which gathered at the juxtanuclear region, are lipid rafts at early endosomes. One possible experiment is to perform the co-fractionation experiment using sucrose density gradient. However, we believe that it would be very difficult to confirm the precise coalescence of APPs with BACE1 in the rafts of "same membrane vesicles". Even if BACE1 and APP were detected at the same fraction, we could not clarify whether these proteins exist at the same membrane vesicles or not. To solve this issue, we need to isolate the membranous structures in the juxtanuclear region and/or to confirm morphologically the co-localization of BACE1/APP in the lipid raft using immuno-electron microscopic analysis. From the morphological data using our light microscopic analysis, all we can say is that a large amount of APP appears to co-localize with BACE1 in the knockdown cells.

Recently, Fernández-Medarde *et al.* (2007) have shown a possible correlation between the decreased expression of CLASP2 and the pathogenesis of AD. They compared the levels of expression of individual genes in the hippocampus of Ras-GRF1 knockout mice, which have defects in memory consolidation, with those in the hippocampus of control mice by using microarray analysis. In this study, the Clasp2 gene was found to be heavily down-regulated and, taken together with the proposed functions of other genes that were found to be expressed differentially in these mice, CLASP2 protein is involved in neurodegenerative diseases such as AD. However, the authors supposed that the decreased expression of CLASP2 might contribute to microtubule destabilization and result in the formation of neurofibrillary tangles by phosphorylating tau during AD pathogenesis. There are few publications to date that demonstrate a positive relationship

among defect in membrane trafficking, decreased activity of GSK3β, and excessive Aβ secretion. Our findings will shed light on the effect of the defect in membrane trafficking on AD pathogenesis.

We found that CDC42BPB, PRKACA, and CSNK2A1 did not enhance Aβ secretion even though they all perturbed the retrograde transport of CI-M6PR between the endosomes and the TGN. This suggests that a defect in the trafficking pathway is not sufficient for the increased secretion of Aβ. The trafficking pathways that are affected in CDC42BPB-, PRKACA-, or CSNK2A1-knockdown cells may be involved in the pathogenesis of diseases other than AD. Further studies are necessary to connect the kinases with their related diseases.

Our novel screening and analytical system has several notable features. Firstly, we will be able to identify the essential pathogenetic proteins that are upstream or downstream of the kinase because the protein kinase network has been studied extensively and many useful databases are available for general use. Secondly, the visual screening and assay system that we have described in this article is applicable to various types of localizomics studies. Several systematic screening methods that are based on gene silencing techniques such as RNAi have currently been established. In particular, recent advances in high-throughput imaging techniques and methods for image analysis have allowed morphological changes or dynamic processes such as mitosis and endo/exocytosis to be characterized in great detail by fluorescence microscopy (Pelkmans *et al.* 2005; Balklava *et al.* 2007). Our developed CellTech Station can do cell culture, transfection of siRNAs and plasmids, and indirect immunofluorescence analysis automatically, with the computational programs. It is highly possible that the functions associated with the CellTech Station are suitable for the various localizomics studies. By analyzing the localization of pathogenetically-important proteins, lipids, or mRNAs after the transfection of siRNAs against kinases, phosphatases, or other types of protein using our system, it will be possible to clarify the molecular links that are between the localization of these proteins and other macromolecules and the pathogenic mechanisms of related diseases.

Experimental procedures

Automatic visual screening system using the CellTech Station

To acquire numerous imaging data in a systematic manner, we established an automated high-throughput fluorescence-based cell imaging system using cell array chips. The system consisted of microchamber array chips, automatic sample preparation equipment (the CellTech Station, which was custom-made for us by Nikkyo Technos Co., Ltd), and automatic fluorescence-image acquisition systems (Fig. 1B). Briefly, 48 microchambers (12 × 4) with a diameter of 2.5 mm and an inter-chamber distance of 3.0 mm were arrayed on a black-quartz chip (Fig. 1B). The bottom of each microchamber was made of transparent quartz (thickness, 0.15 mm), which allowed us to detect fluorescence images within the UV range using an oil immersion lens. The CellTech Station was used to do cell culture, transfection of siRNAs and plasmids, and indirect immunofluorescence analysis automatically, using different computational programs.

To acquire images of the cells in the microchambers, we used an INCell Analyzer 1000 system (GE Healthcare Co., Ltd) or LSM510 confocal microscopy system (Carl Zeiss Co., Ltd). The advantage of this system was the ability to obtain multi-colored images of the 48 microchambers at high speed using a ×40 objective lens. By using the automatic sample preparation system, we could minimize the occurrence of discrepancies between the microchambers that were due to operational mistakes caused by human error.

Chemicals, antibodies and plasmids

The kinase inhibitors H-89, 3-methyladenine, and propranolol were purchased from Sigma Aldrich, and other kinase inhibitors from Calbiochem. These inhibitors were diluted to appropriate concentrations in DMSO and stored at −20 °C.

The antibodies that were used for western blotting were as follows: mouse polyclonal anti-CDC42BPB antibody (Abnova), mouse polyclonal anti-PRKACA antibody (Abnova), mouse polyclonal anti-PRKACG antibody (Abnova), rabbit polyclonal anti-CSNK2A1 antibody (BL753; Bethyl Laboratories), rabbit polyclonal anti-GSK3β antibody (Cell Signaling Technology), rabbit polyclonal anti-APP antibody (AB5352; Chemicon), mouse monoclonal anti-human amyloid β antibody (82E1; IBL), mouse monoclonal anti-GAPDH antibody (MAB374; Chemicon). HRP-conjugated anti-mouse and anti-rabbit antibodies from Upstate Biotechnology and Millpore, respectively, were used as secondary antibodies.

The antibodies that were used for immunofluorescence were as follows: rabbit polyclonal anti-CI-M6PR antibody (IBL), mouse monoclonal anti-p230 antibody (BD Biosciences), mouse monoclonal anti-EEA1 antibody (BD Biosciences), mouse monoclonal anti-Lamp2 antibody (H4B4; Developmental Studies Hybridoma Bank, University of Iowa, Iowa City, IA), rabbit polyclonal anti-myc antibody (Cell Signaling). The mouse monoclonal anti-LBPA antibody was a gift from Dr. Toshihide Kobayashi (RIKEN). The anti-CLASP2 polyclonal antibody was a gift from Dr. Irina Kaverina (Vanderbilt University Medical Center). Cy2- and Cy3-conjugated anti-mouse antibodies (Chemicon), a Cy3-conjugated anti-rabbit antibody (Chemicon), and an Alexa 488-conjugated anti-rabbit antibody (Invitrogen) were used as secondary antibodies.

The VSVGts045-GFP construct was a gift from Dr. Jennifer Lippincott-Schwartz (National Institutes of Health, Bethesda, MD).

Cell culture and transfection

HEK293 cells that stably expressed APPsw, and HeLa cells were cultured in Dulbecco's Modified Eagle's Medium (DMEM; Nissui) supplemented with 10% fetal bovine serum (GIBCO) and penicillin/streptomycin (GIBCO). Geneticin (1 mg/mL; Invitrogen) was also required for the HEK293 stable transfectant. For plasmid transfection into the kinase-knockdown cells, cells that had been incubated for 48 h after transfection with the siRNAs were transfected with 1 μg/mL plasmid using Lipofectamine PLUS (Invitrogen) according to the manufacturer's instructions.

RNAi manipulations

For siRNA screening, knockdown of the kinases by RNAi was carried out by the reverse transfection method using siPORT *NeoFX* Transfection Agent (Ambion) and 30 nM siRNA (*Silencer*® Human Kinase siRNA Library V3; Ambion) according to the manufacturer's instructions. Briefly, a mixture of Transfection Agent and siRNA was aliquotted into the eight-well glass-based dishes (Nunc). Subsequently, HeLa cells (approximately 10 000 per well) were added to the wells. After incubation at 37 °C with 5% CO_2 for 72 h, the cells were immunostained with the antibodies as described in the text.

For the various assays that used kinase-knockdown cells, HeLa cells or HEK293 cells were plated on 35 mm dishes (Nunc) and transfected with 50 nM siRNA using Lipofectamine 2000 (Invitrogen) according to the manufacturer's instructions. The cells were analyzed after 72 h using an LSM510 laser scanning confocal microscope (Carl Zeiss Co., Ltd).

Quantification of Aβ

HEK-APP cells were plated on poly-L-lysine-coated six-well dishes (Sigma-Aldrich). After transfection of the siRNAs for 72 h, the cells were washed with PBS and then fresh medium was added. After a further incubation for 6 h, the medium and cells were collected. Quantification of Aβ in the medium was carried out by sandwich ELISA using a Human β Amyloid (1–40) ELISA Kit (Wako) and a Human β Amyloid (1–42) ELISA High Sensitive Kit (Wako), according to the manufacturer's instructions. The concentration of Aβ was normalized against the total protein concentration in the cell lysate as measured by the bicinchoninic acid (BCA) assay (Pierce).

Cholera Toxin Subunit B (CTxB) transport assay

After treatment with siRNA for 72 h, the cells were incubated with 1 μg/mL Alexa 556-conjugated CTxB (Alexa 556-CTxB) in PBS(+) (PBS with 0.9 mM $CaCl_2$ and 0.5 mM $MgCl_2$) on ice for 30 min and then washed with PBS(+) to remove the unbound toxin. After incubation at 37 °C for various periods of time, the cells were washed and fixed. We counted the number of cells in which Alexa 556-CTxB had accumulated in the juxtanuclear region (N_j: juxtanuclear region-labeled cells), and then calculated the percentage of cells in which transport from the PM to the juxtanuclear region had occurred (100 × N_j/total number of transfected cells).

Acknowledgements

Authors thank K. Osaka and Y. Ishii for experimental assistant. This work was supported by a grant from the Ministry of Education, Culture, Sports, Science and Technology of Japan (19657057 to M. M.) and Japan Science Technology Agency (to F. K.).

References

Akhmanova, A., Hoogenraad, C.C., Drabek, K., Stepanova, T., Dortland, B., Verkerk, T., Vermeulen, W., Burgering, B.M., De, Zeeuw, C.I., Grosveld, F. & Galjart, N. (2001) CLASPs are CLIP-115 and -170 associating proteins involved in the regional regulation of microtubule dynamics in motile fibroblast. *Cell* **23**, 923–935.

Arighi, C.N., Hartnell, L.M., Aguilar, R.C., Haft, C.R. & Bonifacino, J.S. (2004) Role of the mammalian retromer in sorting of the cation-independent mannose 6-phosphate receptor. *J. Cell Biol.* **165**, 123–133.

Balklava, Z., Pant, S., Fares, H. & Grant, B.D. (2007) Genome-wide analysis identifies a general requirement for polarity proteins in endocytic traffic. *Nat. Cell Biol.* **9**, 1066–1073.

Cataldo, A.M., Barnett, J.L., Pieroni, C. & Nixon, R.A. (1997) Increased neuronal endocytosis and protease delivery to early endosomes in sporadic Alzheimer's disease: neuropathologic evidence for a mechanism of increased β-amyloidogenesis. *J. Neurosci.* **17**, 6142–6151.

Cheng, T.S., Hsiao, Y.L., Lin, C.C., Yu, C.T., Hsu, C.M., Chang, M.S., Lee, C.I., Huang, C.Y., Howng, S.L. & Hong, Y.R. (2008) Glycogen synthase kinase 3β interacts with and phosphorylates the spindle-associated protein Astrin*. *J. Biol. Chem.* **283**, 2454–2464.

Conde, S., Pérez, D.I., Martínez, A., Perez, C. & Moreno, F.J. (2003) Thienyl and phenyl α-halomethyl ketones: new inhibitors of glycogen synthase kinase (GSK-3β) from a library of compound searching. *J. Med. Chem.* **46**, 4631–4633.

Dangi, S. & Shapiro, P. (2005) Cdc2-mediated inhibition of epidermal growth factor activation of the extracellular signal-regulated kinase pathway during mitosis. *J. Biol. Chem.* **280**, 24524–24531.

Derby, M.C., Lieu, Z.Z., Brown, D., Stow, J.L., Goud, B. & Gleeson, P.A. (2007) The trans-Golgi network golgin, GCC185, is required for endosome-to-Golgi transport and maintenance of Golgi structure. *Traffic* **8**, 758–773.

Efimov, A., Kharitonov, A., Efimova, N., Loncarek, J., Miller, P.M., Andreyeva, N., Gleeson, P., Galjart, N., Maia, A.R., McLeod, I.X., Yates, J.R., Maiato, H., Khodjakov, A., Akhmanova, A. & Kaverina, I. (2007) Asymmetric CLASP-dependent nucleation of noncentrosomal microtubules at the trans-Golgi network. *Dev. Cell* **12**, 917–930.

Ehehalt, R., Keller, P., Haass, C., Thiele, C. & Simons, K. (2003) Amyloidogenic processing of the Alzheimer β-amyloid precursor protein depends on lipid rafts. *J. Cell Biol.* **160** 113–123.

Fernández-Medarde, A., Porteros, A., de, las, Rivas, J., Núñez, A., Fuster, J.J. & Santos, E. (2007) Laser microdissection and microarray analysis of the hippocampus of Ras-GRF1 knockout mice reveals gene expression changes affecting signal transduction pathways related to memory and learning. *Neuroscience* **146**, 272–85.

Fumoto, K., Hoogenraad, C.C. & Kikuchi, A. (2006) GSK-3b-regulated interaction of BICD with dynein is involved in microtubule anchorage at centrosome. *EMBO J.* **25**, 5670–5682.

Ghosh, P., Griffith, J., Geuze, H.J. & Kornfeld, S. (2003) Mammalian GGAs act together to sort mannose 6-phosphate receptors. *J. Cell Biol.* **163**, 755–766.

Gomes, E.R., Jani, S. & Gundersen, G.G. (2005) Nuclear movement regulated by Cdc42, MRCK, Myosin, and Actin flow establishes MTOC polarization in migrating cells. *Cell* **121**, 451–463.

Hattori, C., Asai, M., Onishi, H., Sasagawa, N., Hashimoto, Y., Saido, T.C., Maruyama, K., Mizutani, S. & Ishiura, S. (2006) BACE1 interacts with lipid raft proteins. *J. Neurosci. Res.* **84**, 912–917.

He, X., Li, F., Chang, W.P. & Tang, J. (2005) GGA proteins mediate the recycling pathway of Memapsin 2 (BACE). *J. Biol. Chem.* **280**, 11696–11703.

Hirosako, K., Imasato, H., Hirota, Y., Kuronita, T., Masuyama, N., Nishioka, M., Umeda, A., Fujita, H., Himeno, M. & Tanaka, Y. (2004) 3-Methyladenine specifically inhibits retrograde transport of cation-independent mannose 6-phospate/insulin-like growth factor II receptor from the early endosome to the TGN. *Biochem. Biophys. Res. Commun.* **316**, 845–582.

Kar, S., Poirier, J., Guevara, J., Dea, D., Hawkes, C., Robitaille, Y. & Quirion, R. (2006) Cellular distribution of insulin-like growth factor-II/mannose-6-phosphate receptor in normal human brain and its alteration in Alzheimer's disease pathology. *Neurobiol. Aging* **27**, 199–210.

Kierbel, A., Gassama-Diagne, A., Mostov, K. & Engel, J.N. (2005) The phosphoinositol-3-kinase–protein kinase B/Akt pathway is critical for *Pseudomonas aeruginosa* strain PAK internalization. *Mol. Biol. Cell* **16**, 2577–2585.

Lee, Y.S., Paek, K.S., Kang, E.S., Jang, H.S., Kim, H.J., Kang, Y.J., Kim, J.H., Lee, H.T., Lee, J.H., Chang, K.C., Nishinaka, T. & Seo, H.G. (2005) Involvement of nuclear factor kB in up-regulation of aldose reductase gene expression by 12-O-tetradecanoylphorbol-13-acetate in HeLa cells. *Int. J. Biochem. Cell Biol.* **37**, 2297–2309.

Mathews, P.M., Guerra, C.B., Jiang, Y., Grbovic, O.M., Kao, B.H., Schmidt, S.D., Dinakar, R., Mercken, M., Hille-Rehfeld, A., Rohrer, J., Mehta, P., Cataldo, A.M. & Nixon, R.A. (2002) Alzheimer's disease-related overexpression of the cation-dependent mannose 6-phosphate receptor increases Aβ secretion. *J. Biol. Chem.* **277**, 5299–5307.

Mimori-Kiyosue, Y., Grigoriev, I,, Lansbergen, G., Sasaki, H., Matsui, C., Severin, F., Galjart, N., Grosveld, F., Vorobjev, I., Tsukita, S. & Akhmanova, A. (2005) CLASP1 and CLASP2 bind to EB1 and regulate microtubule plus-end dynamics at the cell cortex. *J. Cell Biol.* **168**, 141–153.

Noble, W., Planel, E., Zehr, C., Olm, V., *et al.* (2005) Inhibition of glycogen synthase kinase-3 by lithium correlates with reduced tauopathy and degeneration in vivo. *Proc. Natl Acad. Sci. USA* **102**, 6990–6995.

Pelkmans, L., Fava, E., Grabner, H., Hannus, M., Habermann, B., Krausz, E. & Zerial, M. (2005) Genome-wide analysis of human kinases in clathrin- and caveolae/raft-mediated endocytosis. *Nature* **436**, 78–86.

Phiel, C.J., Wilson, C.A., Lee, V.M. & Klein, P.S. (2003) GSK-3b regulates production of Alzheimer's disease amyloid-β peptides. *Nature* **423**, 435–439.

Rajendran, L., Honsho, M., Zahn, T.R., Keller, P., Geiger, K.D., Verkade, P. & Simons, K. (2006) Alzheimer's disease β-amyloid peptides and released in association with exosomes. *Proc. Natl Acad. Sci. USA* **103**, 11172–11177.

Reddy, J.V., Burguete, A.S., Sridevi, K., Ganley, I.G., Nottingham, R.M. & Pfeffer, S.R. (2006) A functional role for the GCC185 golgin in mannose 6-phosphate receptor recycling. *Mol. Cell. Biol.* **10**, 4353–4363.

Rockenstein, E., Torrance, M., Adame, A., Mante, M., Bar-on, P., Rose, J.B., Crews, L. & Masliah, E. (2007) Neuroprotective effects of regulators of the glycogen synthase kinase-3β signaling pathway in a transgenic model of Alzheimer's disease are associated with reduced amyloid precursor protein phosphorylation. *J. Neurosci.* **27**, 1981–1991.

Saido, T.C. & Iwata, N. (2006) Metabolism of amyloid beta peptide and pathogenesis of Alzheimer's disease. Towards presymptomatic diagnosis, prevention and therapy. *Neurosci. Res.* **54**, 235–253.

Saucerman, J.J., Zhang, J., Martin, J.C., Peng, L.X., Stenbit, A.E., Tsien, R.Y. & McCulloch, A.D. (2006) Systems analysis of PKA-mediated phosphorylation gradients in live cardiac myocytes. *Proc. Natl Acad. Sci. USA* **103**, 12923–12928.

Schermer, B., Höpker, K., Omran, H., *et al.* (2005) Phosphorylation by casein kinase 2 induces PACS-1 binding of nephrocystin and targeting to cilia. *EMBO J.* **24**, 4415–4424.

Scott, G.K., Fei, H., Thomas, L., Medigeshi, G.R. & Thomas, G. (2006) A PACS-1, GGA3 and CK2 complex regulates CI-MPR trafficking. *EMBO J.* **25**, 4423–4435.

Shiba, T., Kametaka, S., Kawaşaki, M., Shibata, M., Waguri, S., Uchiyama, Y. & Wakatsuki, S. (2004) Insights into the phosphoregulation of β-secretase sorting signal by the VHS domain of GGA1. *Traffic* **5**, 437–448.

Small, S.A., Kent, K., Pierce, A., Leung, C., Kang, M.S., Okada, H., Honig, L., Vonsattel, J.P. & Kim, T.W. (2005) Model-guided microarray implicates the retromer complex in Alzheimer's disease. *Ann. Neurol.* **58**, 909–919.

Su, Y., Ryder, J. & Ni, B. (2003) Inhibition of Aβ production and APP maturation by a specific PKA inhibitor. *FEBS lett.* **546**, 407–410.

Tesco, G., Koh, Y.H., Kang, E.L., Cameron, A.N., Das, S., Sena-Esteves, M., Hiltunen, M., Yang, S.H., Zhong, Z., Shen, Y., Simpkins, J.W. & Tanzi, R.E. (2007) Depletion of GGA3 stabilizes BACE and enhances β-secretase activity. *Neuron* **54**, 721–737.

Tomiyama, Y., Waguri, S., Kanamori, S., Kametaka, S., Wakasugi, M., Shibata, M., Ebisu, S. & Uchiyama, Y. (2004) Early-phase

redistribution of the cation-independent mannose 6-phosphate receptor by U18666A treatment in Hela cells. *Cell Tissue Res.* **317**, 253–264.

Waguri, S., Tomiyama, Y., Ikeda, H., Hida, T., Sakai, N., Taniike, M., Ebisu, S. & Uchiyama, Y. (2006) The luminal domain participates in the endosomal trafficking of the cation-independent mannose 6-phosphate receptor. *Exp. Cell Res.* **312**, 4090–4107.

Wang, J.Z., Grundke-Iqbal, I. & Iqbal, K. (2007) Kinases and phosphatases and tau sites involved in Alzheimer neurofibrillary degeneration. *Eur. J. Neurosci.* **25**, 59–68.

Weidemann, A., König, G., Bunke, D., Fischer, P., Salbaum, J.M., Masters, C.L. & Beyreuther, K. (1989) Identification, biogenesis, and localization of precursors of Alzheimer's disease A4 amyloid protein. *Cell* **57**, 115–126.

Wilkinson, S., Paterson, H.F. & Marshall, C.J. (2005) Cdc42-MRCK and Rho-ROCK signalling cooperate in myosin phosphorylation and cell invasion. *Nat. Cell Biol.* **7**, 255–261.

Wittmann, T. & Waterman-Storer, C.M. (2005) Spatial regulation of CLASP affinity for microtubules by Rac1 and GSKb in migrating epithelial cells. *J. Cell Biol.* **169**, 929–939.

Wong, W. & Scott, J.D. (2004) AKAP signaling complexes: Focal points in space and time. *Nat. Rev. Mol. Cell Biol.* **5**, 959–970.

Received: 10 November 2008
Accepted: 30 November 2008

Supporting Information/Supplementary material

The following Supporting Information can be found in the online version of the article:

Figure S1 Validation of the efficiency of gene silencing by RNAi in our system.

Figure S2 The siRNA efficiency of gene silencing in HeLa cells or HEK-APP cells.

Figure S3 Subcellular localization of CI-M6PR in kinase-knockdown HeLa cells.

Figure S4 Effects of GSK3β or CLASP2 knockdown on the retrograde transport of Cholera toxin subunit B (CTxB) from the endosomes to the TGN.

Table S1 List of the kinase inhibitors and their incubation conditions

Table S2 List of the kinase siRNAs

Additional Supporting Information may be found in the online version of the article.

Please note: Wiley-Blackwell are not responsible for the content or functionality of any supporting information supplied by the authors. Any queries (other than missing material) should be directed to the corresponding author for the article.

Neuron
Article

Mechanism of Ca^{2+} Disruption in Alzheimer's Disease by Presenilin Regulation of $InsP_3$ Receptor Channel Gating

King-Ho Cheung,[1] Diana Shineman,[2,4] Marioly Müller,[1] César Cárdenas,[3] Lijuan Mei,[1] Jun Yang,[1] Taisuke Tomita,[5] Takeshi Iwatsubo,[5] Virginia M.-Y. Lee,[2,4] and J. Kevin Foskett[1,3,*]
[1]Department of Physiology
[2]Department of Pathology and Laboratory Medicine
[3]Department of Cell and Developmental Biology
[4]Center for Neurodegenerative Disease Research
University of Pennsylvania, Philadelphia, PA 19104, USA
[5]Department of Neuropathology and Neuroscience, University of Tokyo, Tokyo 113-0033, Japan
*Correspondence: foskett@mail.med.upenn.edu
DOI 10.1016/j.neuron.2008.04.015

SUMMARY

Mutations in presenilins (PS) are the major cause of familial Alzheimer's disease (FAD) and have been associated with calcium (Ca^{2+}) signaling abnormalities. Here, we demonstrate that FAD mutant PS1 (M146L) and PS2 (N141I) interact with the inositol 1,4,5-trisphosphate receptor ($InsP_3R$) Ca^{2+} release channel and exert profound stimulatory effects on its gating activity in response to saturating and suboptimal levels of $InsP_3$. These interactions result in exaggerated cellular Ca^{2+} signaling in response to agonist stimulation as well as enhanced low-level Ca^{2+} signaling in unstimulated cells. Parallel studies in $InsP_3R$-expressing and -deficient cells revealed that enhanced Ca^{2+} release from the endoplasmic reticulum as a result of the specific interaction of PS1-M146L with the $InsP_3R$ stimulates amyloid beta processing, an important feature of AD pathology. These observations provide molecular insights into the "Ca^{2+} dysregulation" hypothesis of AD pathogenesis and suggest novel targets for therapeutic intervention.

INTRODUCTION

Alzheimer's disease (AD) is a common dementia involving slowly developing and ultimately fatal neurodegeneration. Most AD is sporadic and usually develops at age >60, but ~10% of AD is inherited as an autosomal-dominant trait (familial AD, FAD) and disease develops as early as the late 30 years of age. Mutations in amyloid precursor protein (APP) and presenilins (PS1, PS2) cause early onset FAD (Hutton and Hardy, 1997). Hallmark features of AD include accumulations of extracellular β amyloid (Aβ) plaques and intracellular neurofibrillary tangles with neuronal atrophy or loss (Hardy, 2006; Mattson, 2004). The "amyloid hypothesis" of AD postulates that accumulation of oligomeric or fibrillar Aβ, due to production of more amyloidogenic forms of Aβ and defective processing and clearance, leads to pathological sequelae associated with the disease (Haass and Selkoe, 2007; Hardy and Selkoe, 2002). This hypothesis has nevertheless been questioned (De Strooper, 2007; Hardy and Selkoe, 2002; Shen and Kelleher, 2007), and others have also been proposed to describe pathological origins of the disease (reviewed in Blennow et al., 2006; Mattson, 2004). Accumulating evidence suggests that sustained disruption of intracellular Ca^{2+} signaling may play an early proximal, and perhaps central, role in AD pathogenesis (Gandy et al., 2006; LaFerla, 2002; Mattson and Chan, 2003; Smith et al., 2005a; Stutzmann, 2005). Ca^{2+} is involved in many facets of neuronal physiology, including activity, growth and differentiation, synaptic plasticity, and learning and memory, as well as pathophysiology, including necrosis, apoptosis, and degeneration (Berridge et al., 2000). Before identification of PS, Ito (Ito et al., 1994) discovered that fibroblast lines derived from AD patients, later shown to harbor the A246Q mutation in PS1, without exception, generated exaggerated intracellular Ca^{2+} concentration ($[Ca^{2+}]_i$) responses to submaximal concentrations of two G protein-coupled receptor (GPCR) agonists that activate phospholipase C (PLC). Activation of GPCR, including bradykinin, $5HT_{2A}$ and metabotropic glutamate receptors, stimulates PLC activity that produces inositol 1,4,5-trisphosphate ($InsP_3$), which binds to its receptor ($InsP_3R$), an endoplasmic reticulum (ER)-localized Ca^{2+} channel, resulting in release of Ca^{2+} from the ER and elevation of $[Ca^{2+}]_i$ (Foskett et al., 2007). Enhanced Ca^{2+} release could not be attributed to altered amounts of Ca^{2+} in the ER or number of agonist receptors or to plasma membrane influx pathways (Ito et al., 1994). It was suggested that alteration of $InsP_3R$-mediated Ca^{2+} release was a fundamental defect in AD, although the molecular mechanisms were undefined. Subsequently, it was demonstrated that enhanced $InsP_3$-mediated Ca^{2+} signaling was a highly predictive diagnostic feature of AD-derived peripheral cells (Hirashima et al., 1996). Many subsequent studies have confirmed that mutant PS expression is associated with exaggerated ER Ca^{2+} release in several cellular and animal model systems including cells from FAD patients (Etcheberrigaray et al., 1998; Hirashima et al.,

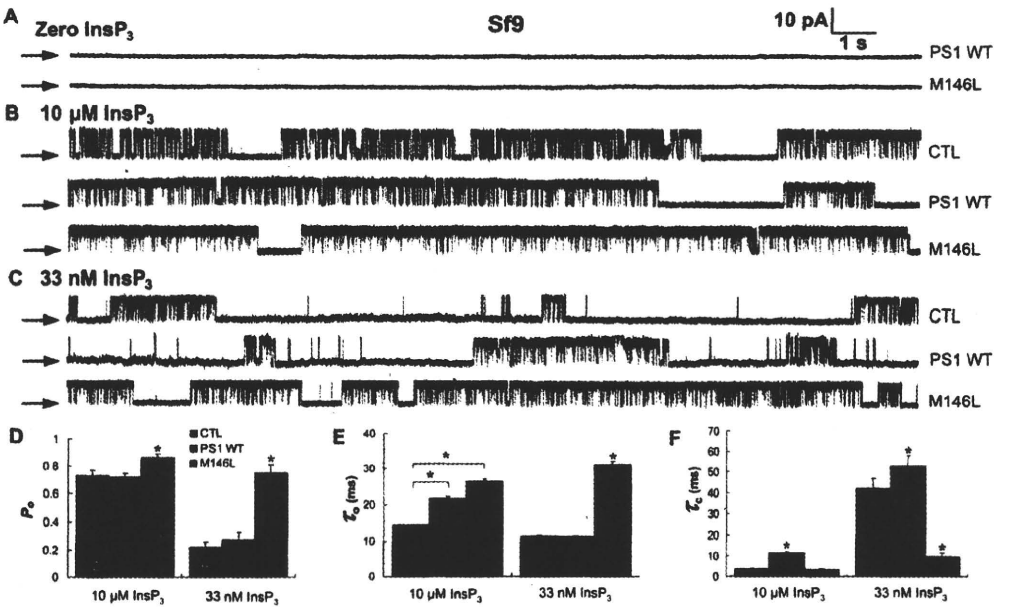

Figure 1. Effects of PS1 Expression on $InsP_3R$ Single-Channel Activity in Sf9 Cells

(A–C) Representative current recordings in isolated nuclei from Sf9 cells infected with PS1 WT or M146L baculoviruses in absence (A) or presence of saturating (10 μM; B) or subsaturating (33 nM; C) $InsP_3$ in pipette solution. Channel activity was not evoked by PS1 alone in absence of $InsP_3$ (A), whereas $InsP_3R$ channels were activated in presence of $InsP_3$ (B and C). Pipette $[Ca^{2+}]$ was 1 μM; arrows: zero current level. Summary of effects of PS1 expression on $InsP_3R$ channel open probability P_o (D) mean open time (τ_o) (E) and mean closed time (τ_c) (F). Bars indicate standard error of the mean. Asterisks: $p < 0.01$, unpaired t test. Data presented in Table S1.

1996; Ito et al., 1994), neuronal and nonneuronal cells engineered to express recombinant mutant PS proteins (Cedazo-Minguez et al., 2002; Guo et al., 1996; Johnston et al., 2006; Leissring et al., 1999a, 1999b, 2001; Smith et al., 2002) and cells from mutant PS transgenic animals (Leissring et al., 2000), including brain neurons (Barrow et al., 2000; Mattson et al., 2000; Schneider et al., 2001; Stutzmann et al., 2004, 2006) long before the appearance of plaques and tangles (Stutzmann et al., 2004). A "Ca^{2+} overload" hypothesis has been widely invoked to account for exaggerated Ca^{2+} release in mutant PS-expressing cells (discussed in Stutzmann, 2005), but increased ER Ca^{2+} stores have not been consistently observed (Giacomello et al., 2005; Ito et al., 1994; Lessard et al., 2005; Zatti et al., 2004, 2006) nor is there a consensus regarding possible molecular mechanisms involved (Gandy et al., 2006; LaFerla, 2002; Smith et al., 2005a; Stutzmann, 2005). Here, we have discovered a mechanism that can account for intrinsic altered Ca^{2+} signaling in AD cells that involves a biochemical and functional interaction of WT and FAD mutant PS with the $InsP_3R$ Ca^{2+} release channel. The biochemical interactions of FAD mutant PS1 or PS2 with the $InsP_3R$ profoundly enhance the activity (gating) of the channel that results in and can account for exaggerated cellular Ca^{2+} signaling. By use of $InsP_3R$-deficient cells, we show that this enhancement is directly involved in mutant PS-mediated APP processing (Aβ generation), an important feature of AD pathology (Mattson and Guo, 1997).

RESULTS

Modulation of $InsP_3R$ Channel Activity by PS1 in Sf9 Cells

The effects of PS expression on $InsP_3R$ channel activity were examined in native ER membranes by single-channel patch-clamp electrophysiology of the outer membrane of isolated Sf9 cell nuclei (Ionescu et al., 2006). Insect cells express a single $InsP_3R$ isoform, most closely related to the mammalian type 1 channel, the predominant brain isoform (Foskett et al., 2007), that has permeation and gating properties and ligand regulation very similar to those of mammalian $InsP_3R$ channels (Ionescu et al., 2006). In membrane patches from control nuclei, $InsP_3R$ channels exposed to optimal ligand conditions (10 μM $InsP_3$, 1 μM Ca^{2+}) were consistently detected, and they gated with high open probability ($P_o = 0.76 \pm 0.05$, n = 10; Figure 1B and see Table S1 available online). Human wild-type PS1 (PS1-WT) and FAD mutant PS1 M146L (PS1-M146L) were expressed in Sf9 cells as full-length holoproteins (Figure S1) throughout the ER (not shown) and in the nuclear envelope (Figure S2). In nuclei from either FAD mutant PS1-M146L- or PS1-WT-expressing cells, no novel ion channels were detected (n = 59; Figure 1A). Nor were channel activities observed in the absence of $InsP_3$ (n = 10; Figure 1A) or in the presence of $InsP_3$ together with its competitive inhibitor heparin (100 μg/ml; n = 7; not shown). $InsP_3R$ channels observed in the presence of saturating 10 μM $InsP_3$ in membrane patches

from PS1-WT-infected cells had P_o similar to those from mock-infected or uninfected cells ($p > 0.05$; Figures 1B and 1D). In contrast, P_o was elevated ($p < 0.05$) in PS1-M146L-infected cells ($P_o = 0.86 \pm 0.03$; Figures 1B and 1D), with many channels observed to be "locked open" for long periods (as in Figure 1B), a gating behavior only extremely rarely observed in control channels (unpublished data). PS1-M146L enhanced $InsP_3R$ gating in saturating [$InsP_3$] by prolonging the channel open time (Figure 1E). Interestingly, PS1-WT also enhanced the mean open time, although to a lesser extent than mutant PS1 (Figure 1E), and it also enhanced the mean closed time (Figure 1F).

With [$InsP_3$] lowered to 33 nM, $InsP_3R$ channel P_o in patches from control nuclei was reduced to 0.27 ± 0.01, reflecting the [$InsP_3$] dependence of gating (Ionescu et al., 2006). Strikingly, P_o was elevated by nearly 3-fold in patches from nuclei isolated from the FAD mutant PS1-expressing cells ($P_o = 0.75 \pm 0.06$), to a level that was comparable to that observed in saturating [$InsP_3$] (Figures 1C and 1D). Enhanced P_o was caused by a marked destabilization of the channel closed state (enhanced opening rate) as well as prolongation of the open time (Figures 1E and 1F). In contrast, PS1-WT was without effect on P_o (Figure 1D); although it appeared to influence channel gating, reflected as a small increase of the channel mean closed time (Figure 1F).

Biochemical Interaction of PS1 with $InsP_3R$

These results demonstrate a gain-of-function effect of mutant PS1 on $InsP_3R$ channel activity observed at the single-channel level. Because the effects of FAD PS1 expression were observed in isolated nuclei, we speculated that this functional effect was caused by an association of PS with the $InsP_3R$ in the ER membrane patches. PS1-WT and PS1-M146L immunoprecipitates from Sf9 cells that had been co-infected with rat types 1 or 3 $InsP_3R$ contained both $InsP_3R$ channel isoforms (Figure 2A). Similarly, PS1 immunoprecipitates from mouse whole brain lysates contained the type 1 $InsP_3R$ (Figure 2C). These results demonstrate a biochemical interaction between $InsP_3R$ and both WT and mutant PS1.

Modulation of $InsP_3R$ Channel Activity by PS1 in DT40 Cells

Similar studies were undertaken in chicken DT40 cells, using analogous protocols, but with polyclonal lines engineered to stably express either WT or mutant PS1 proteins (Figure S3). A DT40 line with all three $InsP_3R$ isoforms genetically deleted ($InsP_3R$-KO DT40) constitutes the only $InsP_3R$ null cell line available (Sugawara et al., 1997). We reasoned that if PS1 similarly affected gating of $InsP_3R$ channels in native $InsP_3R$-expressing DT40 cells, the generality of this as a molecular mechanism associated with FAD mutant PS1 could be established, and furthermore that use of $InsP_3R$-KO DT40 cells would be valuable for investigating the physiological relevance of the PS-$InsP_3R$ interaction. As in the Sf9 cell recordings, no novel ion channel activities were observed in nuclei from the wild-type or mutant PS1-expressing native DT40 cells (not shown). Importantly, highly similar effects of PS expression on $InsP_3R$ channel behavior were observed as in the Sf9 cells (Figure 3; Table S2). Thus, in saturating [$InsP_3$], PS1-WT was without effect ($P_o = 0.53 \pm 0.05$ in control versus 0.57 ± 0.07 in PS1-WT transfected cells), whereas PS1-M146L expression increased channel activity ($P_o = 0.83 \pm 0.04$; $p < 0.01$; Figures 3A and 3C) by locking the channel open for long periods (Figure 3D). In suboptimal [$InsP_3$] (100 nM), mutant PS1 stimulated channel activity by 4-fold ($P_o = 0.63 \pm 0.07$ versus 0.16 ± 0.02 for control cells; Figures 3B and 3C) to levels similar to those observed for control channels in saturating [$InsP_3$]. Also as in Sf9 cells, PS1-WT was without effect on P_o, although it influenced channel gating, as evidenced by small effects on both mean open and closed times (Figures 3D and 3E).

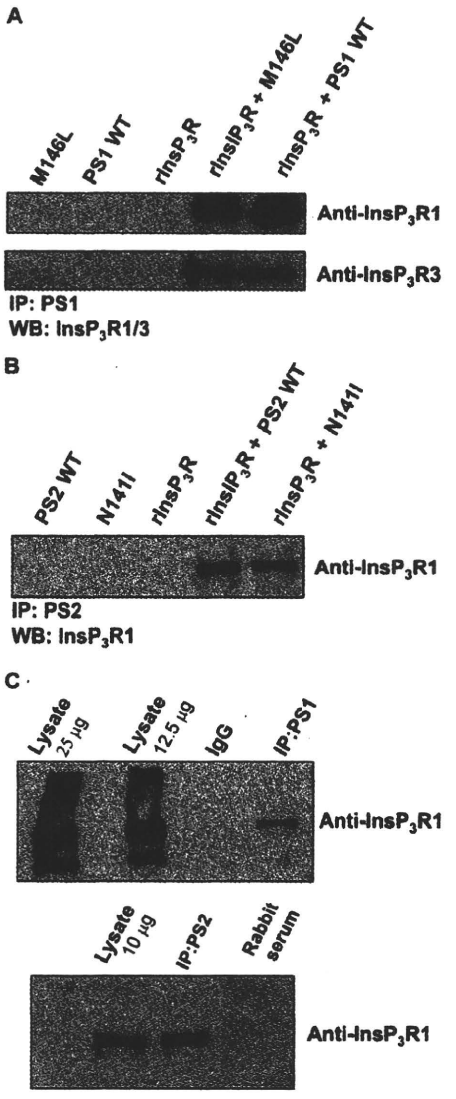

Figure 2. Biochemical Interaction between PS and $InsP_3R$

Western blot of PS1 (A) or PS2 (B) immunoprecipitates from lysates of Sf9 cells coexpressing either PS1-WT or PS1-M146L (A) or PS2-WT or PS2-N141I (B) with rat $InsP_3R$ isoforms 1 or 3; expressed proteins shown at top and probing antibodies shown on right.

(C) Western blots of PS1 (top) and PS2 (bottom) immunoprecipitates from mouse brain lysate. Top: lanes 1 and 2, total input; lane 3, IgG immunoprecipitate control; lane 4, PS1 immunoprecipitate. Bottom: lane 1, total input; lane 2, PS2 immunoprecipitate; lane3, rabbit serum immunoprecipitate control.

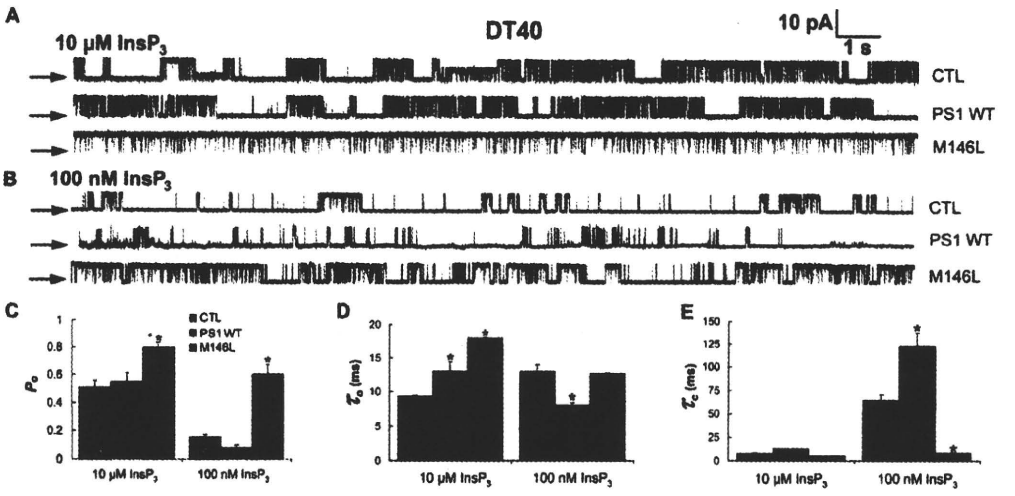

Figure 3. Effects of PS1 Expression on $InsP_3R$ Single-Channel Activity in DT40 Cells

Representative $InsP_3R$ single-channel current recordings in presence of saturating (10 μM; A) or subsaturating (100 nM; B) $InsP_3$ in DT40 cells stably transfected with PS1 WT or M146L. Pipette $[Ca^{2+}]$ was 1 μM, optimal for channel activity; arrows: zero current level. Summary of effects of PS1 expression on $InsP_3R$ P_o (C), mean open time (τ_o) (D), and mean closed time (τ_c) (E). Bars indicate standard error of the mean. Asterisks: $p < 0.01$, unpaired t test. Data presented in Table S2.

The similar behaviors of $InsP_3R$ gating from different species in different cell systems in response to expression of FAD mutant and WT PS1 strongly suggests that this is a fundamental channel regulatory mechanism.

Modulation of $InsP_3R$ Channel Activity by PS2

Altered $[Ca^{2+}]_i$ signaling has been observed in cells expressing either FAD mutant PS1 or PS2 (Gandy et al., 2006; LaFerla, 2002; Smith et al., 2005a; Stutzmann, 2005). Like PS1, wild-type PS2 (PS2-WT) and FAD mutant PS2 N141I (PS2-N141I) also localized to the nuclear envelope (Figure S2) and interacted biochemically with the $InsP_3R$ (Figures 2B and 2C). With 10 μM $InsP_3$ in the pipette solution, $InsP_3R$ channels from PS2-WT-infected cells (Figure S1) had P_o similar to those from mock-infected cells ($p > 0.05$; Figures 4A and 4C; Table S3). In contrast, P_o was elevated ($p < 0.05$) in PS2-N141I expressing cells ($P_o = 0.81 \pm 0.02$; Figure 4C). As observed for PS1-M146L, many channels observed in PS2-N141I nuclei were "locked open" (as in Figure 4A). With subsaturating $[InsP_3]$, P_o in patches from PS2-N141I nuclei was elevated by nearly 3-fold compared with P_o observed in nuclei from mock or PS2-WT-expressing cells (Figure 4C). Similar to the effect of PS1-M146L, elevated P_o was caused primarily by marked enhancement of the opening rate and prolongation of the mean open time (Figures 4D and 4E). PS2-WT was without effect on channel P_o (Figures 4B and 4C), but it influenced gating, reflected as increases in the mean closed and open times (Figures 4D and 4E). These effects of WT and FAD mutant PS2 on $InsP_3R$ gating are highly similar to those observed for WT and mutant PS1, respectively, strongly suggesting that aberrant modulation of $InsP_3R$ channel gating is a general property of FAD mutant PS.

Exaggerated Ca^{2+} Signaling in Mutant PS1-Expressing Cells

To address whether these effects of FAD mutant PS observed at the single-channel level account for altered $[Ca^{2+}]_i$ signaling in AD cells, $InsP_3R$-mediated Ca^{2+} signals were recorded in the DT40 cell lines that were used for the single-channel studies and that had comparable levels of $InsP_3R$ expression (Figure S3). Physiological $InsP_3R$-mediated Ca^{2+} signals were elicited by crosslinking the B cell receptor (BCR). A high concentration of anti-IgM (5 μg/ml) triggered a rapid increase in $[Ca^{2+}]_i$ in control cells (Figure 5A) due to $InsP_3$-mediated Ca^{2+} release from intracellular stores (Sugawara et al., 1997). In PS1-WT-expressing cells, the magnitude and kinetics were similar to those observed in control cells. In contrast, exaggerated $[Ca^{2+}]_i$ responses were observed in PS1-M146L-expressing cells (Figure 5A), with the peak response over 1.5-fold higher than in control or PS1-WT-expressing cells (Figure 5B). Thus, the DT40 cell system recapitulates the exaggerated $[Ca^{2+}]_i$ responses observed in peripheral cells from FAD patients and neuronal and nonneuronal animal and model cells expressing FAD mutant PS. In response to a low anti-IgM concentration (0.05 μg/ml) expected to generate less $InsP_3$, repetitive $[Ca^{2+}]_i$ oscillations were triggered in 52% ± 5% of control cells (Figures 5C and 5D), due to periodic Ca^{2+} release through the $InsP_3R$ (White et al., 2005) after a long lag period (Figure 5F) as $[InsP_3]$ increased to levels sufficient for channel stimulation. In cells expressing PS1-M146L, the peak amplitude of the oscillations was similar to those observed in control and PS1-WT-expressing cells (Figure S4), whereas both the oscillation frequency and number of responding cells were increased, and the latency between application of agonist and the first $[Ca^{2+}]_i$ response was decreased (Figures 5C–5F). Of note, the latency was nearly abolished in

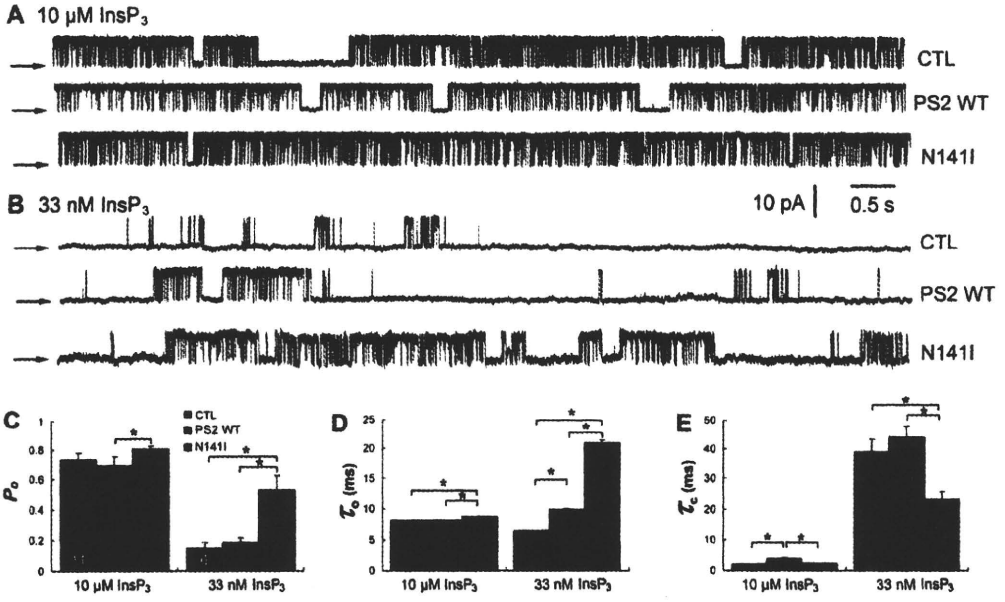

Figure 4. Effect of PS2 on $InsP_3R$ Single-Channel Activity in Sf9 Cells

(A and B) Representative current recordings in isolated nuclei from Sf9 cells infected with PS2 WT or N141I baculovirus in the presence of saturating (10 μM; A) or subsaturating (33 nM; B) $InsP_3$. Pipette $[Ca^{2+}]$ was 1 μM; arrows: zero current level. Summary of effects of PS2 expression on $InsP_3R$ P_o (C), channel mean open time (τ_o) (D), and channel mean closed time (τ_c) (E). Bars indicate standard error of the mean. Asterisks: $p < 0.01$, unpaired t test. Data presented in Table S3.

a significant subset (~30%) of cells expressing PS1-M146L (Figures 5C and 5F). This response is highly reminiscent of that of control cells to saturating concentrations of BCR antibody (Figure 5A) and was never observed in control or PS1-WT-expressing cells. Increased number of oscillating cells, enhanced oscillation frequency and diminished latencies are all consistent with a heightened $InsP_3$ sensitivity of $InsP_3R$-mediated Ca^{2+} release in the FAD mutant PS1-expressing cells. Interestingly, the number of responding cells was increased and the latency was shortened in the PS1-WT-expressing cells (Figures 5D and 5E), although to a lesser extent than the more exaggerated responses observed in cells expressing FAD mutant PS1.

Spontaneous $InsP_3R$-dependent $[Ca^{2+}]_i$ oscillations were observed in ~6% of control cells perfused with Hank's balanced salt solution without stimulation (Figures 5G and 5H), as observed previously (White et al., 2005). Expression of PS1-WT approximately doubled the percentage of cells displaying this behavior (Figure 5H). In contrast, a 4-fold higher percentage, ~25%, of the PS1-M146L-expressing cells exhibited spontaneous $[Ca^{2+}]_i$ oscillations (Figure 5H). Furthermore, the oscillation frequency in these cells was also enhanced (Figure 5I). In a subset of the mutant PS1-expressing cells (~4%), spontaneous exaggerated $[Ca^{2+}]_i$ transients were observed that were never seen in control and PS1-WT-expressing cells (Figure 5G).

These results are congruent with those obtained in the single-channel studies. In both sets of experiments, exaggerated responses to $InsP_3$, particularly under conditions of low $[InsP_3]$, were observed in the context of FAD mutant PS1 expression, with PS1-WT expression also having effects, but much less exaggerated. The congruence of two very different sets of data suggests that the observed exaggerated $[Ca^{2+}]_i$ responses are due to the observed exaggerated $InsP_3R$ single-channel responses.

Exaggerated Ca^{2+} Signaling in Mutant PS1-Expressing Cells is Due to Altered $InsP_3R$ Gating

Exaggerated $[Ca^{2+}]_i$ responses have been a consistent observation in cells expressing mutant PS proteins (LaFerla, 2002; Smith et al., 2005a; Stutzmann, 2005; Yoo et al., 2000), but it has been suggested that they are caused by enhanced expression of release channels (Chan et al., 2000; Kasri et al., 2006; Schneider et al., 2001; Smith et al., 2005b; Stutzmann et al., 2006) or overfilling of ER Ca^{2+} stores (Leissring et al., 2000; Leissring et al., 2001; Schneider et al., 2001; Tu et al., 2006). We therefore examined whether either factor contributed to the exaggerated $[Ca^{2+}]_i$ responses observed here in DT40 cells. All three cell lines expressed approximately equal levels of the types 1 and 3 $InsP_3R$ (Figure S3). Thus, the exaggerated responses cannot be accounted for by altered $InsP_3R$ expression in our studies. To investigate the filling state of intracellular Ca^{2+} stores, we evaluated $[Ca^{2+}]_i$ responses to the Ca^{2+} ionophore ionomycin or the SERCA inhibitor thapsigargin applied in the absence of extracellular Ca^{2+} so that the observed $[Ca^{2+}]_i$ responses were due entirely to Ca^{2+} derived from intracellular compartments. Ionomycin (5 μM) triggered a rapid release of Ca^{2+} that was diminished in the PS1-M146L- but not PS1-WT-expressing cells (Figure S5). Similarly, Ca^{2+} released in response to thapsigargin (1 μM) was also significantly reduced in the mutant

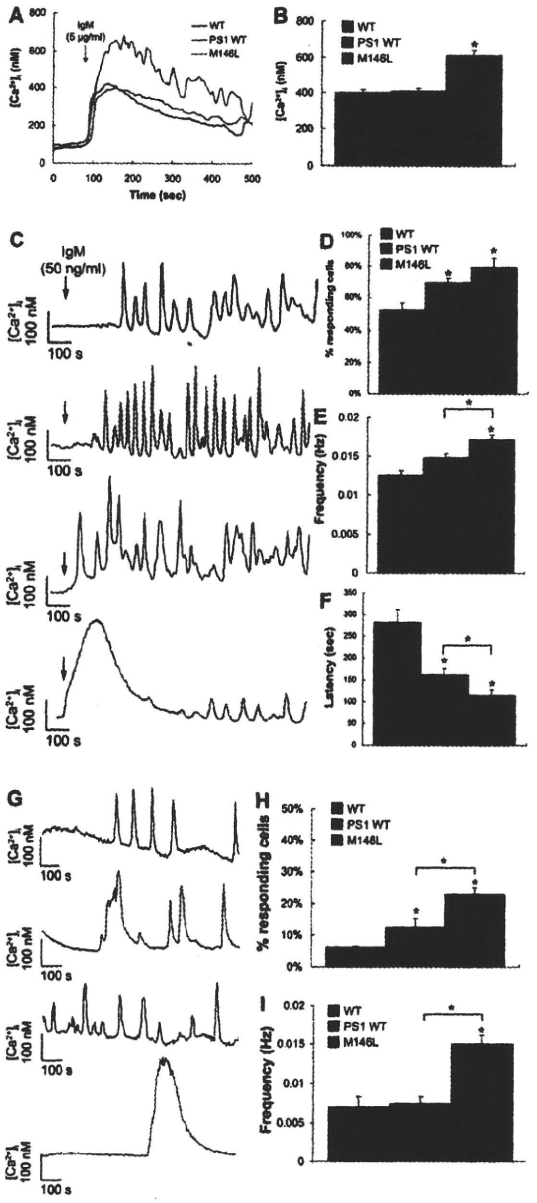

Figure 5. Exaggerated $[Ca^{2+}]_i$ Signaling in Mutant PS-Expressing DT40 Cells

(A and B) Responses to strong stimulation by BCR antibody of DT40 cell $[Ca^{2+}]_i$. (A) Representative single-cell responses to 5 μg/ml anti-IgM (added at arrow) in untransfected (blue) and PS1-WT (red) and PS1-M146L (green) stably-transfected DT40 cells. (B) Summary of peak $[Ca^{2+}]_i$ responses triggered by 5 μg/ml anti-IgM (n = 90). Asterisk: $p < 0.01$ compared with WT and PS1-WT.

(C–F) Responses to weak stimulation by BCR antibody of DT40 cell $[Ca^{2+}]_i$. (C) Representative single cell $[Ca^{2+}]_i$ responses to 50 ng/ml anti-IgM (IgM; added at arrow) stimulation of BCR in control (blue), PS1-WT (red) and PS1-M146L (green and pink) stably transfected DT40 cells. (D) Summary of percentage of cells responding to 50 ng/ml anti-IgM (n = 90). Approximately thirty percent (purple) of PS1-M146L-expressing cells exhibited a different, exaggerated $[Ca^{2+}]_i$ response. (E) $[Ca^{2+}]_i$ oscillation frequency triggered by anti-IgM in WT DT40, PS1-WT-expressing, and PS1-M146L-expressing cells. (F) Summary of latencies to first response in WT DT40, PS1-WT-expressing, and PS1-M146L-expressing cells. The 30% of PS1-M146L-expressing cells that exhibited the exaggerated response had nearly no latency (purple).

(G–I) Spontaneous $[Ca^{2+}]_i$ oscillations in PS1-expressing DT40 cells. (G) Representative spontaneous single-cell $[Ca^{2+}]_i$ oscillations in control (blue) and PS1-WT (red) and PS1-M146L (green and purple) stably transfected DT40 cells. Some PS1-M146L-expressing cells (~4%, purple) displayed a distinct, exaggerated spontaneous $[Ca^{2+}]_i$ signal (bottom). (H) Percentage of cells displaying spontaneous $[Ca^{2+}]_i$ oscillations (n = 90). (I) Spontaneous $[Ca^{2+}]_i$ oscillation frequency observed in WT DT40 cells and PS1-WT- and PS1-M146L-expressing DT40 cells.

Asterisks: $p < 0.01$ compared with WT DT40 cells. Asterisks with bars: $p < 0.01$ PS1-WT versus PS1-M146L. Bars indicate standard error of the mean.

PS1-expressing cells and, to a lesser extent, in the PS1-WT-expressing cells (Figure S5). These results suggest that the Ca^{2+} stores are not overloaded in mutant PS1-expressing cells and may in fact even be reduced. To examine the filling state of the ER Ca^{2+} stores more directly, ER $[Ca^{2+}]$ was measured with the low-affinity fluorescence indicator Mag-Fura-2 (Laude et al., 2005). Addition of MgATP to a solution bathing permeabilized cells with Ca^{2+} stores depleted (not shown) enhanced the fluorescence ratio as a consequence of SERCA-mediated loading of intracellular stores with Ca^{2+} (Figure 6). At steady state, the stores in the FAD PS1-expressing cells were loaded less fully than in control or PS1-WT-expressing cells (Figure 6A; $p < 0.01$), confirming that the Ca^{2+} stores are not overloaded in the mutant PS1-expressing cells. In contrast, when loading was performed in the presence of the $InsP_3R$ inhibitor heparin, the steady-state level of ER Ca^{2+} was similar in all the cell lines (Figure 6B). Thus, the exaggerated $[Ca^{2+}]_i$ responses observed in mutant PS1-expressing DT40 cells (Figure 5) cannot be accounted for by overfilling of ER Ca^{2+} stores. Rather, a reduced ER Ca^{2+} was observed in the FAD-PS1 expressing cells that appeared to be due an activated heparin-sensitive Ca^{2+} leak through the $InsP_3R$. This was more directly examined by use of a different protocol, in which the Ca^{2+} leak permeability of the ER membrane was measured following the addition of thapsigargin to cells with ER stores filled with Ca^{2+} to equivalent levels. The Ca^{2+} leak rate was similar in control and PS1-WT cells, whereas it was greater in the FAD mutant PS1-expressing cells (Figures 6C and 6D). This enhanced Ca^{2+} leak observed in the PS1-M146L cells was eliminated by addition of heparin (Figures 6E and 6F), suggesting that it was mediated by the $InsP_3R$. To test this rigorously, we generated stable PS1-expressing DT40 cells with genetic disruption of all three $InsP_3R$ genes (Sugawara et al., 1997). In the absence of $InsP_3R$ expression (Figure S3), both anti-IgM-induced and spontaneous $[Ca^{2+}]_i$ signals were absent (not shown). Notably, the sizes of the intracellular Ca^{2+} stores in the PS1-M146L- or PS1-WT-expressing cells were similar in the $InsP_3R$-deficient cells (Figure 6G). Importantly, the enhanced PS1-M146L induced ER Ca^{2+} leak rate was absent in the $InsP_3R$-deficient cells (Figure 6H). These results demonstrate that exaggerated Ca^{2+} signaling, reduced Ca^{2+} store size, and enhanced ER Ca^{2+} leak permeability are specific properties of PS1-M146L-expressing cells and, furthermore, that these features are completely dependent on the $InsP_3R$. Together, these results strongly